Earth Planet. Sci. Lett. 641 (2024) 118814

Contents lists available at ScienceDirect

Earth and Planetary Science Letters

journal homepage: www.elsevier.com/locate/epsl

The impact of adsorption–desorption reactions on the chemistry of Himalayan rivers and the quantification of silicate weathering rates

Alasdair C.G. Knight [a,*], Emily I. Stevenson [a], Luke Bridgestock [b], J. Jotautas Baronas [c], William J. Knapp [a], Basanta Raj Adhikari [d], Christoff Andermann [e,f], Edward T. Tipper [a]

[a] Department of Earth Sciences, University of Cambridge, Cambridge, CB2 3EQ, Cambridgeshire, UK
[b] School of Earth and Environmental Sciences, University of St Andrews, St Andrews, KY16 9AJ, Fife, UK
[c] Department of Earth Sciences, Durham University, Durham, DH1 3LE, County Durham, UK
[d] Department of Civil Engineering, Tribhuvan University, Kathmandu, 44613, Bagmati, Nepal
[e] Géosciences Rennes, Université de Rennes, CNRS, UMR 6118, Rennes, 35042, Brittany, France
[f] Helmholtz Centre Potsdam, GFZ German Research Center for Geosciences, Section 4.6: Geomorphology, Potsdam, 14473, Brandenburg, Germany

ARTICLE INFO

Editor: A. Jacobson

Dataset link: https://doi.org/10.5880/fidgeo.2024.008

Dataset link: https://doi.org/10.5880/GFZ.4.6.2023.001

Keywords:
Adsorption-desorption reactions
Silicate weathering
River chemistry

ABSTRACT

Common environmental adsorbents (clay minerals, metal-oxides, metal-oxyhydroxides and organic matter) can significantly impact the chemistry of aqueous fluids via adsorption–desorption reactions. The dissolved chemistry of rivers have routinely been used to quantify silicate mineral dissolution rates, which is a key process for removing carbon dioxide (CO_2) from the atmosphere over geological timescales. The sensitivity of silicate weathering rates to climate is disproportionately weighted towards regions with high erosion rates. This study quantifies the impact of adsorption-desorption reactions on the chemistry of three large Himalayan rivers over a period of two years, utilising both the adsorbed and dissolved phases. The concentration of riverine adsorbed cations are found to vary principally as a function of the concentration and cation exchange capacity (CEC) of the suspended sediment. Over the study period, the adsorbed phase is responsible for transporting ~70% of the mobile (adsorbed and dissolved) barium and ~10% of the mobile calcium and strontium. The relative partitioning of cations between the adsorbed and dissolved phases follows a systematic order in both the monsoon and the dry-season (preferentially adsorbed: Ba > Sr & Ca > Mg & K > Na). Excess mobile sodium (Na* = Na-Cl) to silicon (Si) riverine ratios are found to vary systematically during an annual hydrological cycle due to the mixing of low temperature and geothermal waters. The desorption of sodium from uplifted marine sediments is one key process that may increase the Na*/Si ratios. Accounting for the desorption of sodium reduces silicate weathering rate estimates by up to 83% in the catchments. This study highlights that surficial weathering processes alone are unable to explain the chemistry of the rivers studied due to the influence of hydrothermal reactions, which may play an important role in limiting the efficiency of silicate weathering and hence modulating atmospheric CO_2 concentrations over geological time.

1. Introduction

The dissolution of silicate minerals by carbonic acid is an important chemical reaction for stabilising atmospheric carbon dioxide (CO_2) concentrations over million year timescales (Berner, 1990). This process provides a pathway for the net transfer of carbon from the atmosphere to the hydrosphere (Ebelmen, 1845). The global sensitivity of silicate mineral dissolution rates to climatic factors (e.g., precipitation, temperature) is thought to be disproportionately controlled by highly erosive regions, which are not limited by the supply of water and acids, or shielded by regolith (e.g., Stallard and Edmond, 1987; West et al., 2005; Brantley et al., 2023). The Himalayas is a key example of such a region, where it is postulated that uplift-driven increases in silicate weathering rates reduced atmospheric CO_2 concentrations and surface temperatures during the Cenozoic (Raymo and Ruddiman, 1992). Consequently, numerous studies have focused on the quantification of silicate weathering rates in such regions (e.g., Galy and France-Lanord, 2001; Bickle et al., 2005).

* Corresponding author.
E-mail address: acgk2@cam.ac.uk (A.C.G. Knight).

https://doi.org/10.1016/j.epsl.2024.118814
Received 25 February 2024; Received in revised form 22 May 2024; Accepted 30 May 2024
Available online 14 June 2024

Commonly environmental adsorbents (clay minerals, metal–oxides, metal–oxyhydroxides and organic matter) are capable of modifying the chemistry of aqueous fluids via adsorption-desorption reactions. These phases can be classified as authigenic or detrital depending on their provenance. Authigenic phases form in the modern weathering environment, whereas detrital phases are sourced from the physical weathering of pre-existing rocks. Detrital phases can therefore either be from a previous weathering cycle (and uplifted on to the continents within sedimentary units) or formed during diagenesis/metamorphism. Adsorption-desorption reactions complicate the quantification of chemical weathering rates via the removal or addition of chemical weathering products from solution. For example, contemporary silicate weathering rates are commonly quantified using dissolved sodium measurements corrected for other non-silicate sodium sources (Gaillardet et al., 1999; Moon et al., 2014). A number of studies have highlighted the potential ability of recycled detrital adsorbents to retain sodium during marine burial or contact with saline brines, which rapidly desorbs upon contact with terrestrial waters (Tipper et al., 2020; Cerling et al., 1989). This process provides an alternative source of sodium to rivers—inflating estimates of silicate weathering rates which are typically calculated as a linear function of dissolved sodium concentrations (Galy and France-Lanord, 1999)—leading to an overestimation of atmospheric CO_2 drawdown rates. Furthermore, within highly erosive regions (where the concentration of suspended sediment is often at its greatest) a significant proportion of the dissolved chemical weathering products may be transported by rivers in the adsorbed phase. To identify the impacts of adsorption-desorption reactions on river chemistry, both the adsorbed and dissolved phases (collectively termed *mobile* phases) must be quantified.

In the present study, we provide a time series of mobile cation concentrations collected over a two-year period at a frequency of 2 to 7 days. This allows for a robust quantification of the bias in silicate weathering fluxes in three Himalayan catchments — covering an area of 88 000 km^2 (Fig. 1). These catchments are some of the most rapidly-eroding on Earth (Andermann et al., 2012; Lupker et al., 2012), and are hence pivotal for understanding the relationship between tectonics and atmospheric CO_2 concentrations.

2. Methods

2.1. Localities and samples

A time series of water and suspended sediment samples were collected between 2015 and 2018 from the middle of the channel at the surface of the water column. Collected samples span the entire range of suspended sediment concentration and discharge profiles of the Saptakoshi and Sunkoshi rivers (Fig. 1). Additional paired samples were collected from the Narayani River between 2015 and 2017, from the surface and at depth, using a modified WildCo™ Van Dorn style depth sampler. All paired water–sediment samples were filtered in-situ through 0.22 µm polyethersulfone (PES) membranes. Suspended sediment samples were scraped from the filters to avoid perturbing the chemical composition of the adsorbed phase (Sayles and Mangelsdorf, 1977), before being freeze or oven dried at temperatures of less than 40 °C. An additional 345 water samples, collected at intervals of 1 to 7 days from the Saptakoshi and Sunkoshi rivers, were used to increase the temporal resolution of the dissolved cation data. A time series of previously published discharge measurements, suspended sediment concentrations, and dissolved ion concentrations were used for the Narayani River (Märki et al., 2021; Morin et al., 2018). Daily discharge and suspended sediment concentration measurements from the monsoon period (May-September) and near-daily measurements outside the monsoon period were collected from the Saptakoshi and Sunkoshi rivers.

The sampled rivers are significant tributaries of the Ganges-Brahmaputra river system, the second largest point source of sediment to the oceans (Milliman and Farnsworth, 2013). Notably, all catchments contain a range of lithologies, including uplifted marine sediments present within the Tethyan Sedimentary and Lesser Himalayan Sequences (TSS & LHS; Fig. 1). The denudation rates of the studied catchments range between 0.5 and 2.1 mm yr^{-1} (Andermann et al., 2012; Lupker et al., 2012). This is 9 to 39 times greater than the mean global denudation rate (Wittmann et al., 2020), but is typical of denudation rates across the Himalayas (Andermann et al., 2012; Lupker et al., 2012) and other mountainous regions (Montgomery and Brandon, 2002).

2.2. Identifying biases to the quantification of silicate weathering rates using river chemistry

Field-based silicate weathering rates are commonly quantified by tracing the dissolved products of silicate weathering reactions. Dissolved riverine sodium (Na_{diss}) has been routinely used to quantify global silicate weathering fluxes because it is relatively easily corrected for non-silicate sodium sources (cyclical [c], evaporites [e], anthropogenic pollution [a]) and demonstrates conservative behaviour in most rivers (it is not readily removed from the dissolved phase; e.g., Gaillardet et al., 1999; Moon et al., 2014):

$$Na_{sil} = Na_{diss} - \sum Na_{c,e,a} \tag{1}$$

The dominant non-silicate sodium source is often assumed to be from halite (NaCl) dissolution, such that sodium derived from the dissolution of silicate minerals is given by:

$$Na^* = Na_{diss} - Cl_{diss} \tag{2}$$

Where Cl_{diss} is dissolved chloride. In highly erosive catchments, where suspended sediment concentrations are high, cations bonded to the surfaces of sediment (adsorbed) also become important to quantify (Tipper et al., 2020):

$$Na^* = Na_{diss} + Na_{ad} - Cl_{diss} = Na_{mob} - Cl_{diss} \tag{3}$$

The dissolved and adsorbed phases are collectively termed the *mobile* phase in this study, due to their ability to equilibrate over very short timescales (Sparks, 1986). To test for the impact of sodium desorption on river chemistry, observations of elements commonly released by silicate weathering (Na and Si) were used. For sodic silicate mineral dissolution, in the absence of significant contributions from non-sodium bearing chloride salts (KCl, CaCl, MgCl), it is expected that the ratio of mobile sodium to chloride should be greater than 1:

$$\left(\frac{Na}{Cl}\right)_{mob} > 1 \tag{4}$$

It is also expected that the ratio of Na* (sodium corrected for chloride) to dissolved silicon should be equal to that of the silicate minerals for congruent dissolution:

$$\left(\frac{Na - Cl}{Si}\right)_{mob} = \left(\frac{Na^*}{Si}\right)_{mob} = \left(\frac{Na}{Si}\right)_{sil} \tag{5}$$

The desorption of sodium from recycled detrital adsorbents will increase this ratio via the addition of sodium to fluids.

2.3. Quantifying mobile (adsorbed and dissolved) element concentrations

Element concentration measurements for both phases were performed via inductively coupled plasma optical emission spectroscopy (ICP-OES). Two external certified reference standards (SLRS-6 and SPS-SW2) were repeatedly measured between sample analyses to determine

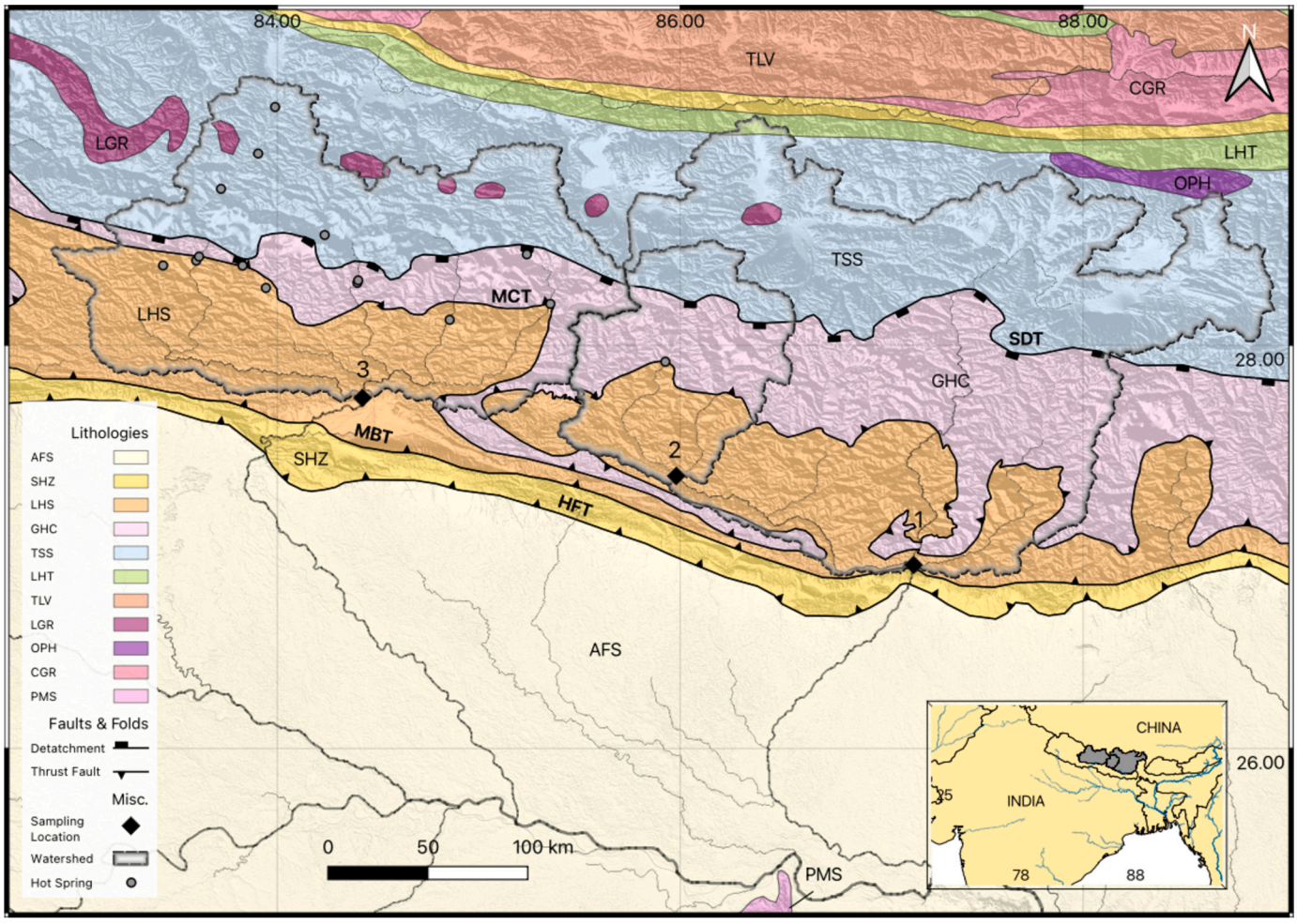

Fig. 1. A simplified geological map of the study catchments. The majority of the samples were collected from stationary sampling sites located on the map by the black diamond markers (1: Saptakoshi River at Chatara; 2: Sunkoshi River at Khurkot; 3: Narayani River at Narayanghat). Known hot spring locations from Evans et al. (2004) and Oliver et al. (2003) are shown via small grey circles. Major lithological units derived from Yin and Harrison, 2000 and Hou et al., 2015 are plotted as follows: Alluvial Floodplain Sediments (AFS); Sub-Himalayan Zone (SHZ); Lesser Himalayan Sequence (LHS); Greater Himalayan Crystalline Complex (GHC); Tethyan Sedimentary Sequence (TSS); Lhasa Terrane (LHT); Tertiary Linzizong Volcanics (TLV); Leucogranite (LGR); Ophiolite (OPH); Cretaceous-Tertiary Granite (CGR); PMS (Proterozoic Metasediments). Uplifted marine sedimentary rocks (including shales) are found within the LHS and the TSS. Major structural features are also shown: Himalayan Frontal Thrust (HFT); Main Boundary Thrust (MBT); Main Central Thrust (MCT); South Tibetan Detachment (SDT).

the uncertainty of element concentration measurements. A breakdown of the precision and accuracy of the standard analyses is provided in the supplementary (Table S.1).

The desorption of adsorbed cations from the suspended sediment was achieved using two independent, well-established methods (ammonium chloride and calcite-saturated hexamminecobalt(III) chloride). Ammonium chloride ($1.0\,mol\,l^{-1}$, Puratronic™ 99.999% metal basis, Thermo Scientific) was selected as a reagent based on its widespread use in soil studies (Sparks et al., 2020). The desorption of an adsorbed ion (X) by NH_4^+ is summarised below, where S represents a negatively charged surface exchange site:

$$NH_4^+ + X{-}S \longrightarrow NH_4{-}S + X^+ \quad (6)$$

Despite its widespread use, the displacement of adsorbed cations by ammonium chloride has been shown to induce carbonate dissolution (Appelo, 1996). To prevent contamination of the adsorbed phase, calcite-saturated hexaamminecobalt(III) chloride (CoHex) was also used (99% metals basis, Sigma Aldrich). CoHex has proved to be an effective reagent for the displacement of adsorbed cations, whilst minimising carbonate dissolution (Lupker et al., 2016; Aran et al., 2008):

$$[Co(NH_3)_6]^{3+} + 3\,X{-}S \longrightarrow [Co(NH_3)_6]{-}S_3 + 3\,X^+ \quad (7)$$

Calcite saturation was achieved by adding $CaCO_3$ powder (99.98%) to CoHex at a concentration of $25.0\,mg\,l^{-1}$. The calcite-saturated CoHex was filtered after a period of 24 hr through 0.22 μm polyethersulfone (PES) membranes to remove excess calcite.

To displace the adsorbed riverine cations, 12.0 ml of reagent ($1.0\,mol\,l^{-1}$ NH_4Cl or calcite-saturated $0.0167\,mol\,l^{-1}$ CoHex) was added to 0.200 g of sediment in an acid-cleaned polypropylene centrifuge tube. The tube was then manually shaken, before being placed in an ultra-sonic bath for 20 min—to ensure the sediment and reagent were thoroughly mixed. The centrifuge tube was then placed on a shaker table for a period of 2 hr. The samples were centrifuged at 3100 g for 30 min to separate the sediment from the supernatant. The supernatant was subsequently transferred via pipette into a separate acid-cleaned centrifuge tube. Another 12.0 ml of reagent was then added to the same sediment sample, and the whole process was repeated to maximise the desorption of sediment-adsorbed riverine cations, whilst minimising the dissolution of sediment. Throughout the procedure, all supernatants were immediately filtered through 0.22 μm PES membrane filters to ensure the effective separation of the sediment and supernatant. The desorption process was performed at room temperature and pressure

(298 K, 1 atm). All reagents used were also at room temperature. Concentrations of abundant, structurally-bound, mineral lattice elements (Al, Fe, and Si) were monitored in the supernatant solutions to identify any potential sediment dissolution occurring during the leaching procedure. Structural cation concentrations were all less than 0.1 $\mu g\,l^{-1}$, suggesting no significant dissolution. Radiogenic strontium isotope measurements of the adsorbed and dissolved phases were also used to confirm samples hadn't been impacted by carbonate dissolution (Fig. S.5).

2.4. The determination of cation exchange capacities (CEC)

The total capacity of the sediment to reversibly adsorb cations (cation exchange capacity, *CEC*) at a fixed set of conditions (e.g., pH, temperature etc.) is an important property of the sediment. Measurements of CEC provide verification that the displacement procedure has been effective—maximising the yield of adsorbed cations whilst minimising the dissolution of solid phases. Evidence about the composition of the adsorbent phases in the sediment can also be deduced from the CEC. Three different measurement methods were used to constrain the CEC of suspended sediment samples: ICP-OES (ammonium chloride), ICP-OES (CoHex) and UV-Vis photospectrometry (CoHex) (section S.1).

2.5. Minimising the bias in temporally limited sampling

The parameters that directly impact mobile cation fluxes (discharge, suspended sediment concentrations and CECs) can vary by orders of magnitude during a single year. To minimise any uncertainty in measured fluxes induced by this natural variability, a time series approach was used to estimate long-term mobile cation fluxes. Observed relationships between discharge, time, and cation concentrations (QTC) were exploited to numerically interpolate the dissolved element data to the same frequency of the discharge and suspended sediment measurements (measured near-daily during the monsoon and every 1 to 4 days during the dry season; figs. S.2 and S.3). To minimise the uncertainty in the models, dissolved cation samples were collected to span the full discharge range. Non-linear regression analyses were subsequently performed to quantify exponents and coefficients for four different QTC models (Table S.3). Adsorption-desorption reaction selectivity coefficients, which describe the partitioning of adsorbed and dissolved cations between the suspended sediment and water, were used to increase the temporal frequency of adsorbed cation measurements (Table S.2). Several different conventions are used in the literature to describe adsorbed cation activities. The Gaines-Thomas convention was adopted due to its thermodynamic consistency and widespread use (Gaines and Thomas, 1953; Townsend et al., 1984). Model uncertainties were propagated using standard Monte-Carlo techniques (section S.3.5).

3. Results

3.1. The variability of mobile cation fluxes

3.1.1. Precipitation driven changes in mobile cation concentrations

During the Indian Summer Monsoon, increased precipitation rates drive greater riverine discharges (Fig. 2a). The largest change is observed in the Saptakoshi, which rises from an average discharge of 640 $m^3\,s^{-1}$ to 2700 $m^3\,s^{-1}$. The Sunkoshi has a slightly lower increase (240 $m^3\,s^{-1}$ to 810 $m^3\,s^{-1}$). Discharge measurements for the Narayani were only available for the monsoon, which has the greatest average discharge during this period (3200 $m^3\,s^{-1}$). The increase in precipitation and discharge mobilises and suspends sediment in the river, increasing sediment concentrations (Fig. 2b). Average suspended sediment concentrations in the Saptakoshi and Sunkoshi increase by a factor of 9 to 10 (0.20 $g\,l^{-1}$ to 1.80 $g\,l^{-1}$ in the Saptakoshi, 0.27 $g\,l^{-1}$ to 2.64 $g\,l^{-1}$ in the Sunkoshi). Suspended sediment concentrations during the monsoon commonly exceed 10 $g\,l^{-1}$, or 20 times the global average (0.5 $g\,l^{-1}$; Milliman and Farnsworth, 2013). Consequently, suspended sediment fluxes are 4 to 5 orders of magnitude greater, increasing from a minimum of 0.03 $t\,day^{-1}$ in the Sunkoshi to a maximum of 24 000 $t\,day^{-1}$ in the Narayani (Fig. 2c). The increase in sediment flux is accompanied by a 2.5 fold increase in the average CEC (2.4 meq/100 g to 5.9 meq/100 g, Fig. 2d). Despite a measurable offset between the seasons, the CECs are highly variable throughout the year with a relative standard deviation of 65% (maximum = 23.5 meq 100 g^{-1}, minimum = 0.7 meq 100 g^{-1}).

The increase in suspended sediment concentrations and CECs during the monsoon increases the concentration of surface sites available for adsorption in the river per unit volume of water (CEC_V) by over an order of magnitude on average (Fig. 3g). This results in the proportion of adsorbed ions being 21-23% of the total mobile concentrations for elements such as calcium and strontium (Fig. 3b&f), and 71% for barium (Fig. 3a). The proportion of cations adsorbed is highly variable throughout the monsoon, varying mostly with suspended sediment concentrations. Calcium and strontium have the largest range in the proportion of cations adsorbed (3% to 84%). Sodium has the smallest range (0 to 42%).

Outside the monsoon period, there is less precipitation and less mobilisation of sediment (0.25 $g\,l^{-1}$ average). The average CEC of the sediment transported is also lower (0.7 meq 100 g^{-1}). Consequently, the concentration of surfaces available for adsorption in the river is greatly reduced (55 $\mu eq\,L^{-1}$; averaged by month then season). Barium is the only element measured that is significantly transported as an adsorbed cation during the dry-season (32% of the mobile Ba, Fig. 3a).

3.1.2. Extreme sediment concentration events: landslides and glacial lake outburst flood events

Transient events with suspended sediment concentrations above 25 $g\,L^{-1}$ are observed in all the rivers. One such event has been identified as a glacial lake outburst flood (GLOF) in the Sunkoshi catchment (Cook et al., 2018) and had a suspended sediment concentration of 47 $g\,L^{-1}$ (Fig. 2b). These events are rarely sampled in chemical weathering studies due to their unpredictable nature and risk to human life. The extreme suspended sediment concentrations result in very high adsorbed to dissolved cation ratios. For example, up to 97% of the mobile barium, and up to 83% of the mobile calcium and strontium, are transported bound to the surfaces of the suspended sediment during these events. Very high suspended sediment fluxes (up to 12 500 $t\,day^{-1}$) result in up to 13% of the annual adsorbed cation budget being transported during extreme events, despite transporting a negligible proportion of the dissolved cation budget (~2%).

3.2. The consistency of mobile cation partitioning between the adsorbed and dissolved phases

Despite large annual variations in discharge, suspended sediment concentrations, and CECs, the relative partitioning of cations between the adsorbed and dissolved riverine phases remains relatively constant (Fig. 3g). The sequence, in order of greatest proportion adsorbed is: $Ba^{2+} > Sr^{2+}$ & $Ca^{2+} > K^{+}$ & $Mg^{2+} > Na^{+}$. This ordering is unchanged despite CEC_V changing by 4 orders of magnitude.

3.3. The long-term adsorbed and dissolved cation budgets

Time-averaged cation concentrations calculated from extensive time series data sets were used to remove bias from temporally limited sampling (Fig. 4, section 2.5). The water and suspended sediment fluxes are dominated by the monsoon, with 80% of the water and 98% of the sediment transported during this period (Fig. 4a). Dissolved cation fluxes are predominantly a function of discharge, whereas adsorbed cation fluxes can be approximated to be directly proportional to suspended sediment fluxes. Consequently, 74% to 100% of the mobile cation budgets are transported during the monsoon. The reduction from direct

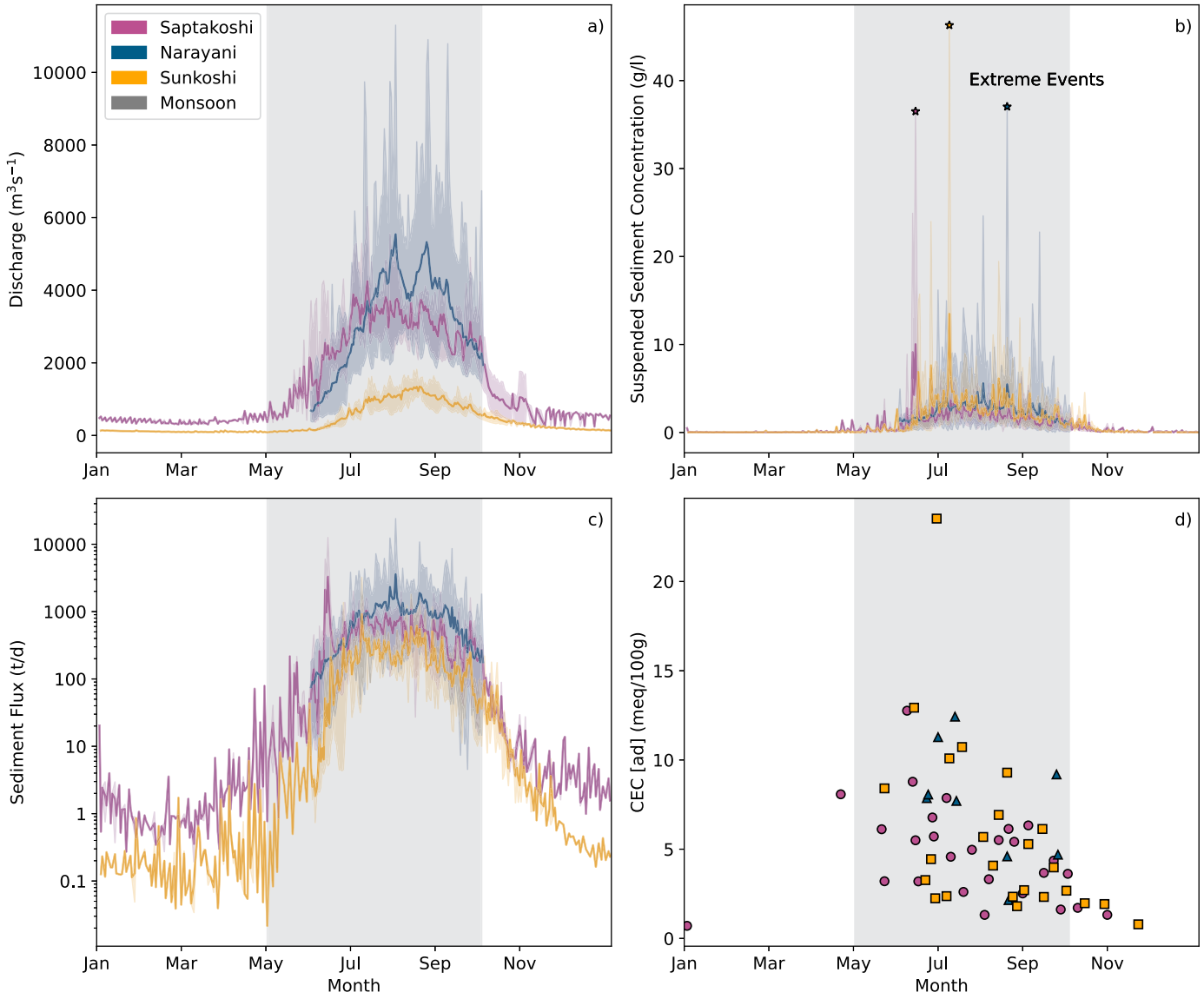

Fig. 2. Minimum, maximum and mean river discharges (a), suspended sediment concentrations (b), suspended sediment fluxes (c) as a function of the time of the year. Sub-figure d) measured cation exchange capacities (CECs) as a function of the time of the year. Extreme sediment concentration events are highlighted on plot b) by star markers. The grey shaded vertical region shows the monsoon period (May-Sept).

proportionality between dissolved cation fluxes and discharge results from the inverse relationship between discharge and dissolved cation concentrations (Fig. S.2). Cation concentrations that increase the most during the dry season (e.g. Na) have a higher proportion (18%) of their dissolved cation budget transported outside the monsoon. Adsorbed cation fluxes are transported exclusively during the monsoon (>98%). The relative importance of the adsorbed budget follows the order observed in Fig. 3. Barium is transported largely in the adsorbed phase. If only dissolved barium concentrations were measured, 71% of the total mobile barium flux would be omitted. Significant proportions of strontium and calcium (11%) are also transported in the adsorbed phase, while sodium, magnesium and potassium are predominantly transported in the dissolved phase (<6% adsorbed, Fig. 4). Using the conventional method of only accounting for the dissolved ions would neglect 10% of the total cation mass flux. The lag between increases in suspended sediment fluxes which peak during July, and discharge which is maximised in August (Fig. 4a), results in July having the greatest ratio of adsorbed to dissolved cations transported for all elements.

3.4. Element concentrations and ratios conventionally used to trace silicate weathering

Mobile sodium and chloride concentrations increase by factors of up to 6 and 10 during the dry season in response to decreases in discharge (Fig. 5). Despite large variations in concentration, Na/Cl ratios do not vary systematically as a function of the time of year (Fig. 6). The greatest difference in Na/Cl ratios is between the rivers, with an average ratio of 2.5 for the Narayani, and 4.9 and 5.6 for the Sunkoshi and Saptakoshi (Fig. 6). Almost all measured Na/Cl ratios (523 out of 526) are greater than the Na/Cl of Himalayan rain (Na/Cl = 1.3; Galy and France-Lanord 2001).

Dissolved silicon (Si) concentrations display a more complex relationship with discharge, following hysteresis loops for annual hydrological cycles in the Saptakoshi and Sunkoshi. Identification of hysteresis in the Narayani is limited due to the absence of dry–season data. Decreasing silicon concentrations are observed during the onset of the monsoon (April-July). Between August and September silicon concentrations increase despite discharge remaining relatively high. Decreases

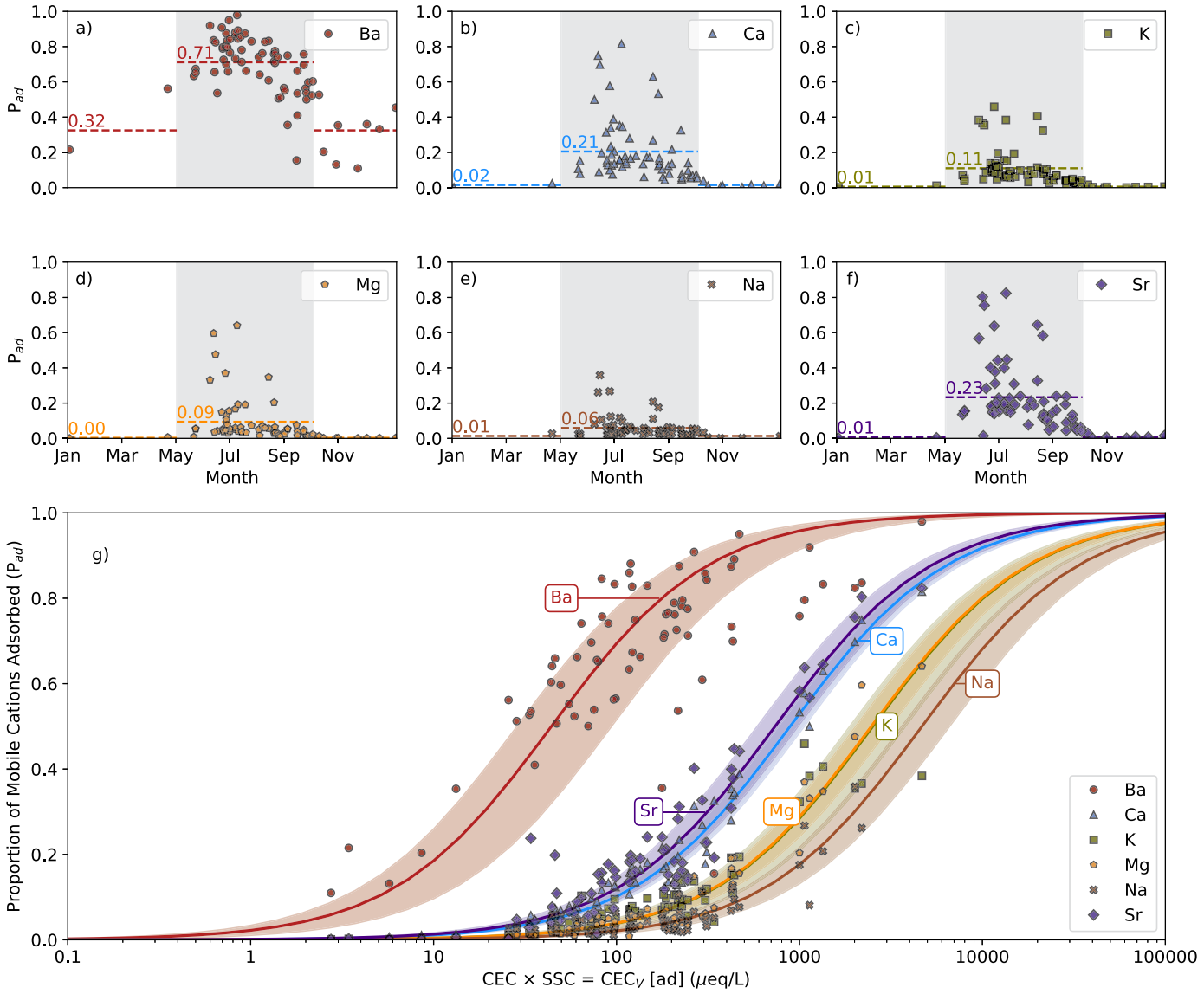

Fig. 3. a-f) The proportion (P) of mobile cations in the adsorbed phase as a function of the month of the year. Mobile cations are defined as the sum of the dissolved and adsorbed cations. Horizontal dashed lines show the mean proportion for the monsoon (grey shaded region) and dry season. g) The proportion of mobile cations in the adsorbed phase as a function of the CEC per unit volume of water (CEC_V). Mass balance models, assuming the proportion of each element adsorbed is a function of the volumetric cation exchange capacity (CEC_V) and a partitioning constant (K), are shown by the solid lines. The shaded region around each model is the standard deviation.

in discharge during October to December result in an increase in silicon concentrations, offsetting concentrations to greater values in comparison to the rising limb data. During January and February silicon concentrations are constant despite falling discharge. All Na*/Si ratios are offset to higher values than the measured Na/Si ratio of plagioclase—the dominant Na-bearing mineral in the catchments (Na/Si = 0.28 ± 0.05 [534]; $\mu \pm \sigma$ [N]). The mean offset is also consistent for the three rivers (0.70 to 0.80). The greatest variability occurs as a function of the time of the year. Minimum ratios of 0.45 are observed during September, while maximum ratios of up to 1.9 are observed in April–May.

4. Discussion & implications

4.1. The applicability of adsorbed cation fluxes to other river systems

Understanding if the adsorbed cation concentrations and fluxes measured in this study are applicable to other river systems requires consideration of the factors which are most likely to impact the partitioning of cations between the adsorbed and dissolved phases: suspended sediment concentrations, CECs, and the relative affinity of competing cations for the adsorbed phase. Suspended sediment concentrations vary by three orders of magnitude and are the main driver of variability in adsorbed cation concentrations (Fig. 3g). The average suspended sediment concentrations measured are greater than the global average, but consistent with rivers draining other mountainous regions (annual average of the three rivers: 0.7 to 2.4 $g\,l^{-1}$; global average: 0.5 $g\,l^{-1}$; Milliman and Farnsworth, 2013). The positive global relationship between riverine suspended sediment concentrations and erosion rates implies mountainous regions are likely to have a disproportionate impact on global adsorbed cation fluxes. The seasonal variability observed in the riverine transit of mobile cations is driven by precipitation. Other regions characterised by large precipitation-driven changes in suspended sediment concentrations will have significant seasonal changes in riverine adsorbed cation concentrations and fluxes. Transient events that induce highly elevated suspended sediment concentrations (GLOFS, landslides and earthquakes) are naturally associated

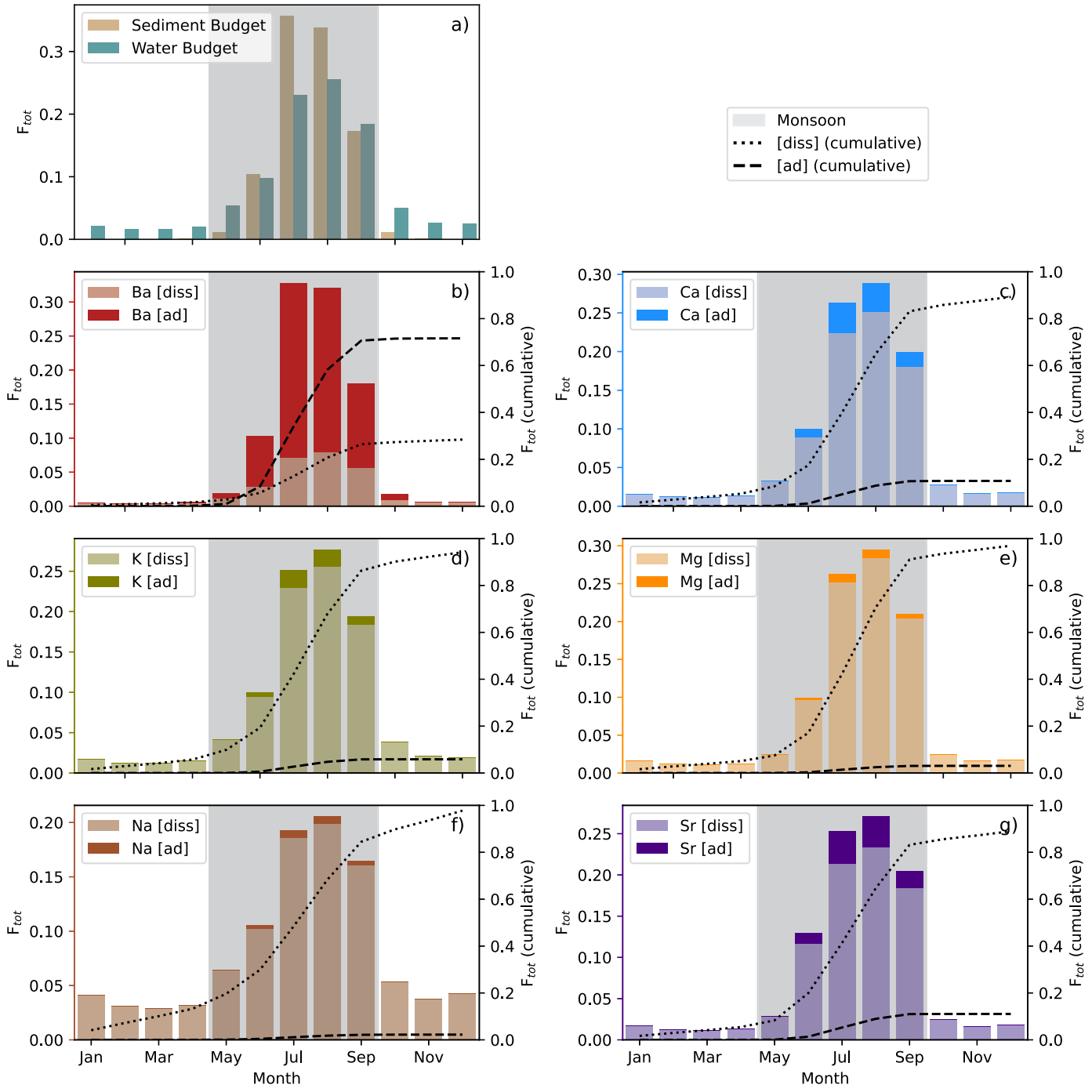

Fig. 4. The proportion of the total annual fluxes a) water (discharge) and suspended sediment, b-g) mobile cations, as a function of the month of the year. The left-hand axis shows magnitude of the proportion and corresponds to the bar plot. The sum of all the bars is equal to one. The right-hand axis displays the cumulative proportions and corresponds to the continuous line plots. The cumulative proportions sum to one at the end of the year.

with mountainous regions, implying the high concentrations and fluxes of adsorbed cations associated with these events are likely to be commonplace throughout these regions.

The CEC of riverine suspended sediment provides a second order control on the adsorbed cation concentrations of this study (Fig. 3g). The CEC of suspended sediment samples from this study are almost all lower than the global average of other large river systems (15 meq 100 g^{-1}; Tipper et al., 2020), but within uncertainty of the CECs measured further downstream in the Ganges-Brahmaputra Basin (Lupker et al., 2016). Producing a predictive framework to understand adsorbed cation fluxes is complicated by the non-linear relationship between CECs and erosion rates. For example, the Amazon River transports a similar proportion of its mobile cation budget in the adsorbed phase to the rivers of this study (12% of Ca and 8% of Mg; Sayles and Mangelsdorf, 1979), despite suspended sediment concentrations being a factor of five lower on average (0.18 $g\,l^{-1}$, Hartmann et al., 2019). This is due, in part, to the Amazon having an average CEC that is five times greater than the rivers of this study. Linear relationships between the CEC and grain size (estimated using the ratio of aluminium to silicon) of suspended sediment have been observed within rivers (Lupker et al., 2016; Tipper et al., 2020), but substantial differences between riverine relationships suggest grain size is

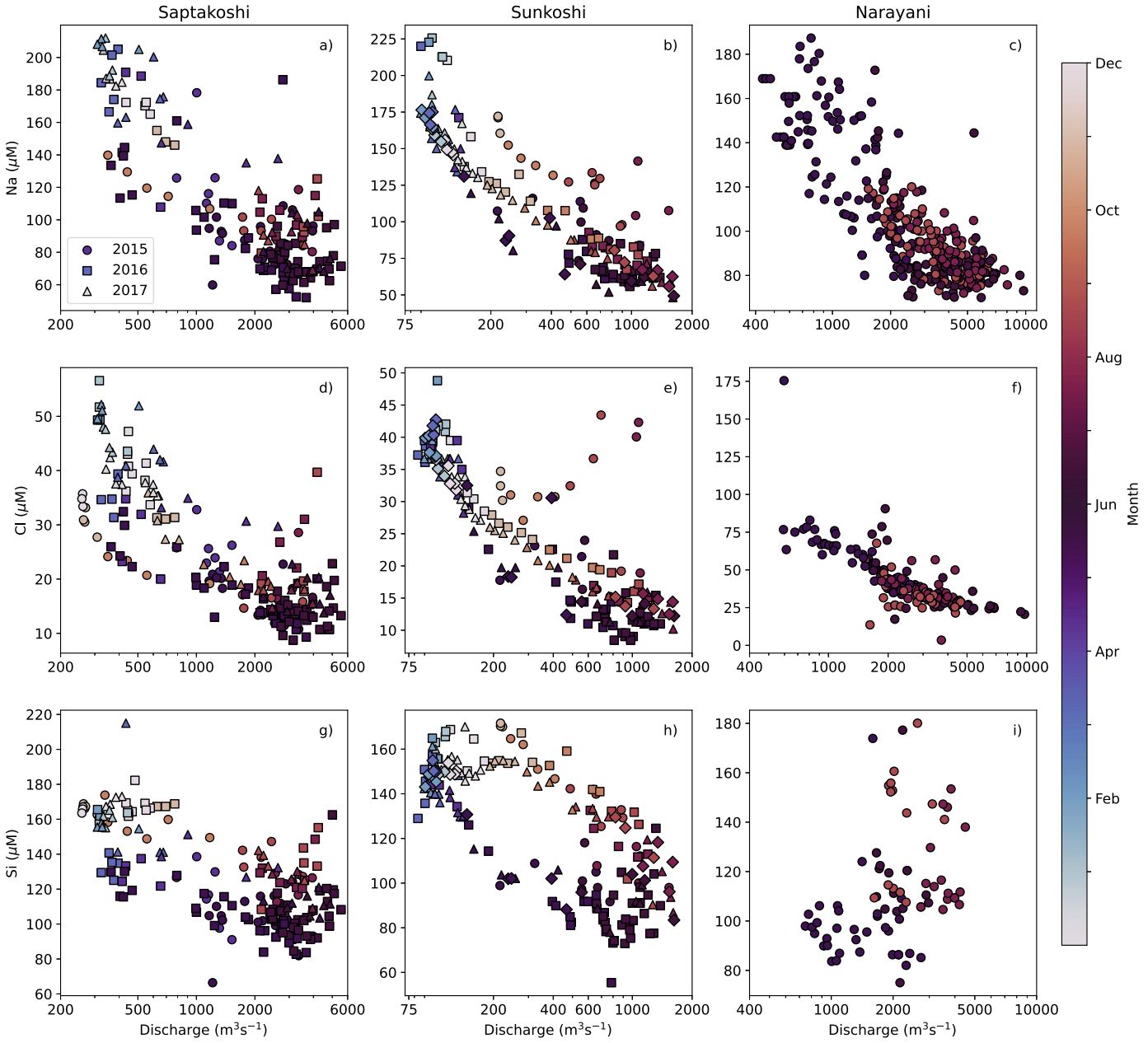

Fig. 5. Mobile (dissolved and adsorbed) element concentrations (Na, Cl, Si) as a function of discharge. Individual years are denoted by different markers: circles (2015), squares (2016), triangles (2017). A colour map has been applied to the markers as a function of the day of the year.

not the only controlling factor. The seasonal variability in the CEC of suspended sediment samples implies the composition and/or size varies systematically throughout the year. Redox-driven changes in the CEC of sediment have previously been observed in seasonally flooded soils (Favre et al., 2002). Similar redox-driven changes may be occurring within the catchments of this study. Variability in the source of suspended sediment provides another potential driver for the seasonal variability observed. Cation exchange capacities are known to vary within weathering profiles as function of depth (White et al., 2009). Increases in the depth of the water table during the monsoon could result in the export of sediment with a higher average CEC. Alternatively, variability in the contribution of sediment from different areas of the catchment may drive the seasonal changes observed.

The relative selectivity of cations for the adsorbed or dissolved phases imposes a third-order control on cation partitioning in this study. There are multiple parameters that are known to impact the relative partitioning of elements between these phases (e.g., pH, ionic strength, Eh, adsorbent composition, temperature etc.); however, spot-samples collected from nine other large river systems indicate a similar partitioning order (Table S.5). This implies that amongst large rivers, the relative partitioning of cations is partially predictable. This consistency potentially derives from the integrative nature of large rivers which have a narrower range of chemical conditions and greater mixing of suspended sediment phases than the smaller tributaries and streams from which they form.

The adsorbed cation flux delivers a chemically unique source of cations to the world's floodplains and oceans. Transient events which drastically increase sediment fluxes (GLOFS and landslides) pose a short-term risk to humans but also provide a long-term benefit via the increased supply of bio-available metal nutrients to flood plains. Globally, sediment fluxes are already undergoing large anthropologically-driven perturbations due to varied human impacts. For example, sediment trapping in head-water regions has reduced global sediment fluxes

to 49% of their pre-dam conditions, while erosion resulting from land use changes in downstream regions has increased sediment concentrations by 41% compared to the 1980s (Dethier et al., 2022). The positive relationship between the fluxes of adsorbed cations and suspended sediment implies that adsorbed cation fluxes have been altered by a similar magnitude, with largely unknown consequences for ecosystems that rely on them. The results from this study highlight the impact of sediment transport dynamics on mobile cation fluxes, underscoring the importance of this understudied aspect of environmental change.

4.2. Exploring the temporal variability in Na*/Si ratios

The excess sodium to silicon ratios (Na*/Si) measured in this study demonstrate an annual cyclicity in all catchments, reaching maximum values during April (~1) and minimum values during September (~0.5). This cyclicity is driven by a decoupling in the behaviour of mobile silicon compared with sodium and chloride in response to discharge (Fig. 5). Silicon displays an anticlockwise hysteresis pattern in the Saptakoshi and Sunkoshi rivers with respect to time. Hysteresis in the discharge-concentration relationships of dissolved riverine elements can be caused by the mixing of water masses with different time-dependent concentration changes (Bouchez et al., 2017). To explain the seasonal temporal variability observed in Na*/Si ratios, mixing of at least two water masses is required (Na*/Si > 1.25 and Na*/Si < 0.45; excluding extreme outliers). Hot springs are common throughout the Himalayas (Evans et al., 2004), dominantly located along thrust faults such as the Main Central Thrust (MCT), and are present in all the catchments of this study (Fig. 1). These geothermal waters have total dissolved solids (TDS) up to 7000 mg l^{-1} (Evans et al., 2004; Oliver et al., 2003). The chemical composition of the waters are largely dominated by sodium (Na^+), bicarbonate (HCO_3^-) and chloride (Cl^-). The vast majority (38 out of 48) of the springs measured have Na/Cl ratios above 1, with an average of Na*/Si ratio of 11 (only inclusive of hot-springs with Na/Cl > 1; Evans et al., 2004; Oliver et al., 2003). The use of dissolved germanium (Ge) as a tracer of hot spring inputs to rivers by Evans et al. demonstrated that geothermal waters can have a significant impact on the chemistry of Himalayan rivers. The impact of geothermal waters has also been more widely recognised within the Ganges-Brahmaputra Basin (Samanta and Dalai, 2016), highlighting the widespread nature of these inputs across the Himalayas in regions with high geothermal gradients and extensive thrust faulting. The range in Na* and Si concentrations measured in the rivers studied (Fig. 6d) are similar to those measured in the headwaters of the Andes (Na* = 25 to 190 μmol l^{-1}, Si = 100 to 240 μmol l^{-1}; Stallard and Edmond, 1987). The variation in dissolved Na*/Si ratios of river waters within the Amazon Basin has been suggested to be driven by surficial weathering rates. The mixing of hydrothermal fluids and surface waters provides an alternative explanation for the variable Na*/Si ratios observed within mountainous regions.

4.3. Sodium addition or silicon removal as the primary driver of the increased Na*/Si ratios

The 2 to 6 fold increase in riverine sodium to chloride ratios (Na/Cl) compared to rain requires either the addition of sodium or removal of chloride from the rivers (Eq. (4), Fig. 6). Chloride is commonly regarded as one of the least reactive elements at low dissolved concentrations, indicating the addition of sodium from a non-halite source is a more likely explanation. The dissolution of sodic silicate minerals is a certain contributor to the excess sodium; however, the ratio of excess sodium to dissolved silicon (Na*/Si) of the rivers is greater than the sodium to silicon ratio (Na/Si) of all primary silicate minerals within the catchment (notably offset by 0.16 to 1.10 from plagioclase—the most abundant sodic silicate mineral with the greatest Na/Si ratio, see Fig. S.6). This offset is even more pronounced for hot springs, which have Na*/Si ratios of up to 80 (Evans et al., 2004). A process is therefore required to explain either the addition of sodium or removal of silicon from the waters.

4.3.1. Hydrothermal secondary silicate mineral precipitation in hot springs

The precipitation of secondary silicate minerals provides a mechanism for the removal of dissolved silicon and the increase in Na*/Si ratios. For the geothermal waters to obtain the elevated Na*/Si ratios observed, virtually all of the silicon released during the dissolution of primary silicate minerals has to be removed from solution (Evans et al., 2004). Provided the study catchments are at steady-state, the export of precipitated Si-rich minerals is also required to explain the continual offset observed. Rivers export the majority of physical weathering products from the continents, so are likely to transport the secondary silicate minerals responsible for the elevated ratios. The clay mineral assemblage of the Sunkoshi and Narayani riverine sediments is dominated by illite/chlorite (75 to 85%; Huyghe et al., 2011). The origin of these clay minerals is considered to be detrital, with variations in illite crystallinity and apatite-fissure tracking (AFT) reflecting a gradient in peak burial temperatures increasing from less than 60 °C in the Western Himalayas to 200 °C in the Easter Himalayas (Vögeli et al., 2017). The illitisation of smectite (I/S) begins between 75 to 120 °C (De Segonzac, 1970) and therefore the proportion of illite derived from I/S is also likely to increase from West to East. The high proportion of detrital clay minerals is in agreement with estimates of sediment recycling factors using lithium isotopes (Dellinger et al., 2014). Kaolinite comprises 5-10% of the clay within the river sediments and is considered to be authigenic (Huyghe et al., 2011). Kaolinite is abundant at Earth's surface and forms from the dissolution of plagioclase ($Na_{0.8}Ca_{0.2}Al_{1.2}Si_{2.8}O_8$, N = 534). The dissolution of plagioclase followed by the precipitation of kaolinite yields an Na*/Si ratio 0.5, which is unable to explain 91% of the river water samples or the geothermal waters. This is also a conservative estimate, as all other silicate minerals measured in the catchments have lower Na/Si ratios (Fig. S.6). To obtain fluid Na*/Si ratios above 0.5, the precipitation of more Si-rich clay mineral phases and/or closed-system behaviour are required. Within the catchment rivers, smectite comprises 5-10% of the total clay abundance, with any remaining proportion comprised of vermiculite (Huyghe et al., 2011). Constraining the impact of smectite precipitation on solution chemistry is challenging due to a wide range of solid-solution compositions. The maximum proportion of clay (per unit mass of suspended sediment) can be constrained to 18% by combining literature estimates for clay mineral CECs (Appelo and Postma, 2005) with the average CEC of the riverine samples (5.5 meq/100 g), of which 14% is detrital and 4% is neoformed. This calculation provides a maximum estimate, as it does not account for other significant environmental adsorbents (metal–oxides, metal–oxyhydroxides and organic matter) which are also likely to be present within riverine suspended sediment samples, suggesting the true proportion of clay is lower. Thermodynamic equilibrium modelling of Himalayan geothermal fluids during ascent indicates the precipitation of secondary silicate phases following decompression and cooling is likely (Becker et al., 2008). The precipitation of Si-rich secondary minerals within hydrothermal fluids provides a potential process to explain the offset between the Na*/Si ratios of fluids and the primary minerals within the catchments.

The assumption that secondary silicate minerals transported by the rivers will be responsible for the increase in fluid Na*/Si ratios is founded on the catchments being at steady-state with respect to clay mineral precipitation and exports. The samples measured in this study span over two years of continuous measurements with no change outside of analytical uncertainty; however, surficial clay precipitation rates are potentially too slow to resolve changes over the study period (Price et al., 2005). Given the high erosion rates of the catchments (corresponding to a minimum denudation rate of 0.5 mm yr^{-1}; Lupker et al., 2012), it is unlikely that secondary silicate minerals formed close to the surface can remain there for substantial periods of time.

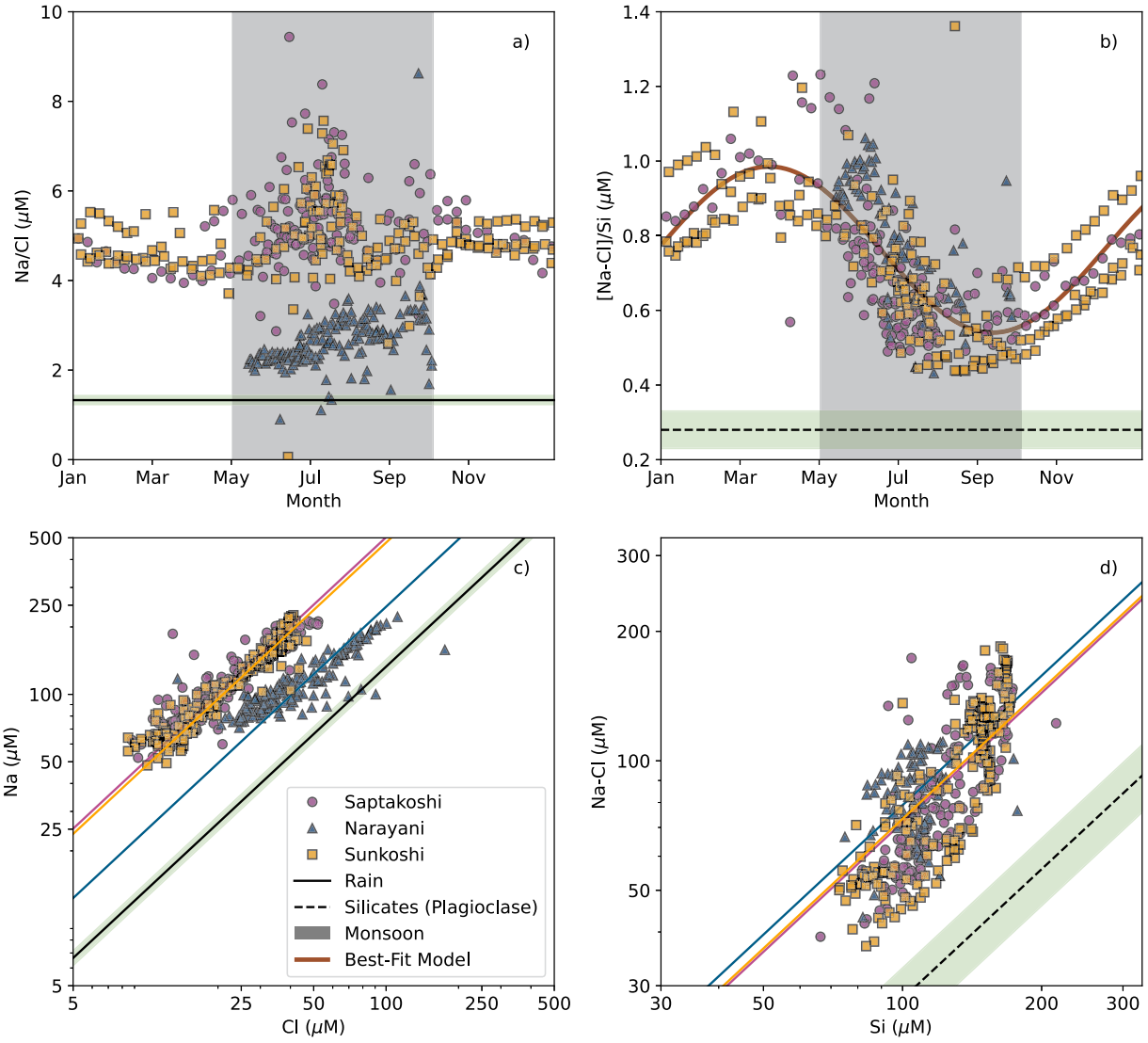

Fig. 6. a) The mobile Na/Cl of river waters plotted as a function of the month of the year. b) The mobile Na*/Si of river waters plotted as a function of the month of the year. A sinusoidal model (y = A.sin(Bx-C)+D) was fitted to the data via a non-linear least-squares regression (SciPy curve-fit). c) Mobile Na concentrations plotted as a function of mobile Cl concentrations. d) Mobile Na* (Na-Cl) concentrations of river water samples plotted as a function of mobile Si concentrations. The average Na/Cl of rain samples (Galy and France-Lanord, 1999) from the Himalayas are displayed, along with the mean Na/Si of the plagioclase samples collected from the Saptakoshi and Sunkoshi ($Na_{0.8}Ca_{0.2}Al_{1.2}Si_{2.8}O_8$, N = 534). Green shaded regions show the standard deviation. The monsoon is shown by the grey vertical shaded portion of the plot.

4.3.2. The desorption of sodium from uplifted marine sediments

An alternative driver of the increased Na*/Si ratios observed is the desorption of sodium from recycled marine sediments, which has previously been suggested to be important in highly erosive catchments (Tipper et al., 2020). Both laboratory experiments and field samples demonstrate that the adsorbed phases of clay minerals and mixed sediments are dominated by sodium when in contact with seawater or sodium–rich brines (Sayles and Mangelsdorf, 1977; Zaytseva, 1958). During the formation of the Himalayas, marine sediments were uplifted to form extensive sedimentary units (LHS & TSS; Yin, 2006; Fig. 1).

To constrain the impact of marine sodium desorption (Na_{de}) on the chemistry of the rivers, the difference in the adsorbed sodium concentration between the modern river sediment (Na_{ad}, determined by direct measurement) and uplifted marine sediment (Na_{up}) was first determined. The flux was then calculated from the product of the difference in sodium concentration and the erosion rate (E, erosion rate estimates from Andermann et al., 2012; Lupker et al., 2012):

$$Na_{de} = (Na_{up} - Na_{ad}) \times E \quad (8)$$

The concentration of riverine adsorbed sodium (Na_{ad}) was measured directly from the suspended sediment samples (section 2.3). The concentration of uplifted adsorbed marine sodium (Na_{up}) was estimated using measurements of the equivalent fraction of sediment-adsorbed sodium at the time of contact with saline fluids ($\beta_{Na\ [m]}$) and the CEC, modified to account for a reduction in the concentration during burial and uplift (F_{rec}):

$$Na_{up} = F_{ad} \times CEC = F_{rec} \times \beta_{Na\ [m]} \times CEC \quad (9)$$

The fraction of the CEC occupied by old marine sodium ($F_{rec} \times \beta_{Na}$) is simplified to F_{ad}. The additional sodium provided by desorption can explain a maximum of 83% of the excess annual dissolved sodium (Na*) observed in the rivers, with any remaining sodium assumed to derive from the dissolution of Na-bearing silicate minerals. The desorption of sodium from uplifted marine sediments (Na_{de}) provides a source of sodium that would be conventionally attributed to silicate weathering if not corrected for (Eq. 2):

$$Na^{**} = Na_{mob} - Cl_{diss} - Na_{de} \quad (10)$$

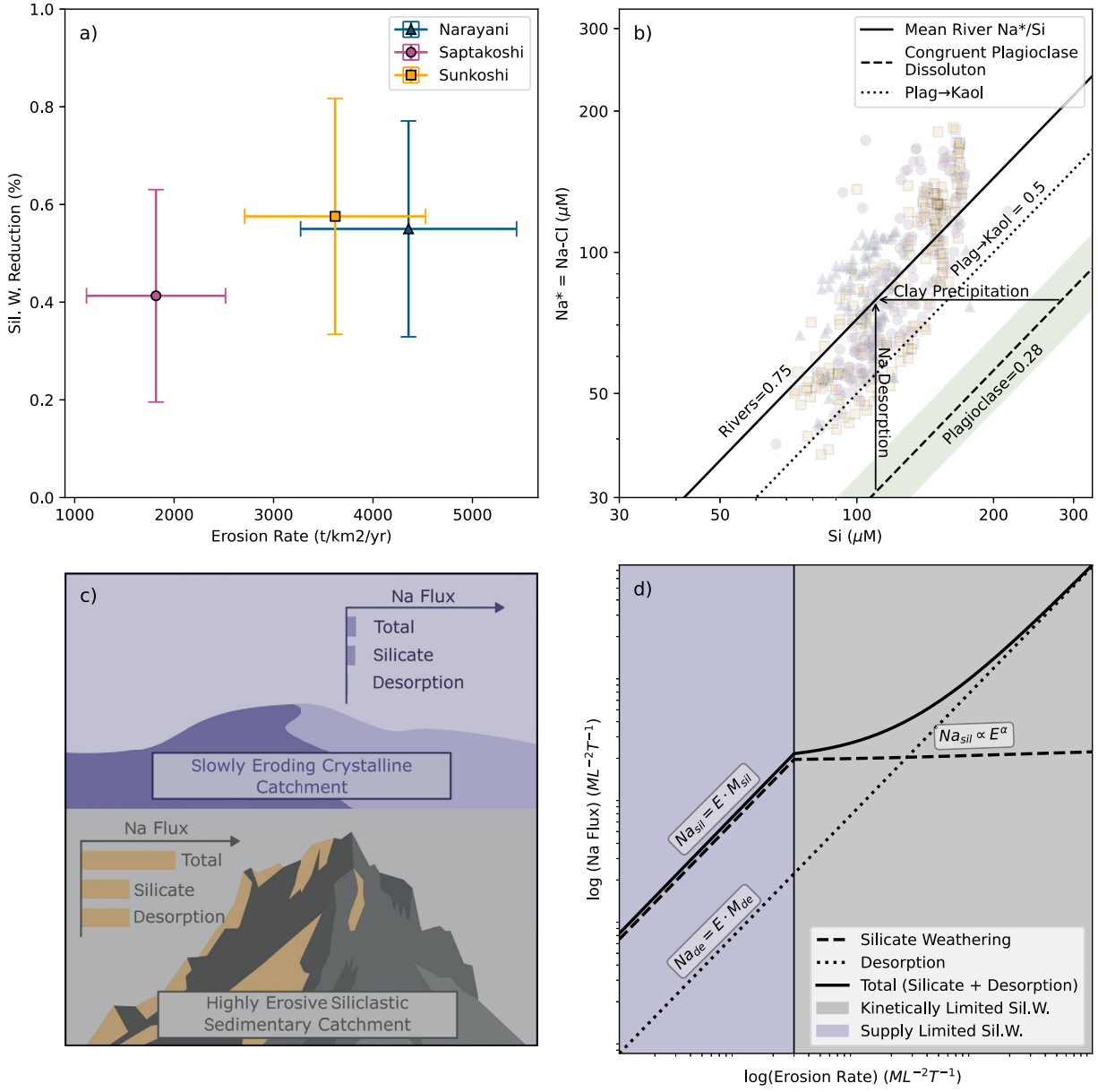

Fig. 7. a) The estimated reduction in silicate weathering fluxes in the study catchments plotted against the average catchment erosion rate. Catchment erosion rates are from Andermann et al. (2012) and Lupker et al. (2012). Error bars display the standard deviation. b) Measurements of mobile riverine Na concentrations, corrected for Cl (Na^*), as a function of the dissolved Si concentrations. Also shown are the Na/Si of the plagioclase measurements (the dominant Na-bearing silicate mineral) from the Saptakoshi and Sunkoshi catchments. The approximate vectors for the change in Na^*/Si ratios during sodium desorption and clay precipitation are represented by the black arrows. c) A comparison of silicate weathering and sodium desorption rates in a catchment with low erosion rates and no uplifted marine siliclastic sediments and one with high erosion rates and abundant uplifted marine siliclastic sediments. d) A simple conceptual model of sodium fluxes across a range of erosion rates (E). Units are expressed as mass per length squared per time ($ML^{-2}T^{-1}$).

The resulting overestimation of silicate weathering fluxes is therefore quantified as:

$$Silicate\ Weathering\ Reduction\ (\%) = \frac{Na_{de}}{Na^*} \times 100 \tag{11}$$

Correcting for sodium desorption from uplifted marine sediments (Na_{de}) reduces conventional silicate weathering rates by 19% to 83% in the studied catchments (Fig. 7a). The Saptakoshi catchment has the greatest predicted reduction ($\mu = 58\%$), followed by the Narayani ($\mu = 54\%$) and the Saptakoshi ($\mu = 42\%$).

The substantial uncertainty in silicate weathering rate reduction estimates chiefly stem from a poor understanding of the fate of adsorbed ions during the burial and uplift of marine sediment. The two parameters used to calculate the fraction of the CEC occupied by old marine sodium during uplift (F_{ad}, Eq. (9)) are: 1) the equivalent fraction of sodium initially adsorbed to sediments during contact with saline waters ($\beta_{Na[m]}$) and 2) the proportion of sodium that remains adsorbed during burial and uplift (F_{rec}). The range in $\beta_{Na[m]}$ values (0.37 to 0.58) are calculated based on the mean and standard deviation of available $\beta_{Na[m]}$ literature values derived from both laboratory experiments and field studies (Sayles and Mangelsdorf, 1977; Zaytseva, 1958). The proportion of sediment from a detrital origin was determined to be between 60% and 85% using stable lithium isotope ratios of modern riverine sediment (Dellinger et al., 2014).

The overestimation of silicate weathering depends on the relative fluxes of sodium from silicate dissolution and desorption, which are primarily a function of lithology and differing reaction kinetics. Adsorption-desorption reactions are rapid (Tang and Sparks, 1993),

therefore desorbed sodium fluxes can be approximated as a linear function of the erosion rate (E) and the adsorbed sodium concentration (M_{de}). Silicate weathering rates are orders of magnitude slower (White and Brantley, 2003). Only at lowest erosion rates (mineral supply limited regions) are silicate weathering rates able to keep pace with erosion. Consequently, the correction to silicate weathering fluxes in supply-limited regions should depend on lithology (Fig. 7d). Only recycled siliclastic sedimentary lithologies contain phases capable of adsorbing meaningful quantities of sodium (shale CECs vary between 1 and 14 meq/100 g; Saidian et al., 2016). The concentration of silicate sodium in shales is variable, but commonly ranges between 1 to 3 wt% Na_2O (Campbell and Williams, 1965). Consequently, the maximum potential correction to silicate weathering in a mineral supply-limited catchment is 20%. At increased erosion rates, silicate minerals pass through the weathering zone with a greater degree of incomplete dissolution, increasing the physical export of silicate minerals. This reduces the slope of the relationship between silicate weathering and erosion in kinetically-limited regions (West et al., 2005), and should increase the relative flux of desorbed sodium to silicate-derived sodium. Lithologies rich in recycled marine sediments are also commonly found in regions with high erosion rates, further increasing the potential correction (European Alps, Southern Alps, Andes, Rockies; Hartmann et al., 2009; Fitzsimons and Veit, 2001; Horton, 2018.

According to the above framework, the proportion of desorbed sodium should increase with both erosion rate and the proportion of recycled marine sediments. Riverine and stream samples collected from Southern Taiwan (Bufe et al., 2021) are found to have greater Na*/Si ratios compared to samples from this study, consistent with greater erosion rates (3 to 6 mm yr^{-1}, Dadson et al., 2003). A number of similarities are also observed between the catchments of Southern Taiwan and this study. Geothermal waters released from hot-springs within the uplifted marine sediments have highly enriched Na*/Si ratios (29 ± 24 (N = 16); $\mu \pm \sigma$) and are largely composed of Na^+ and HCO_3^- (Jang et al., 2012), potentially suggesting variability observed within the riverine samples may also relate to hot-spring proximity and activity. The clay mineralogy of these catchments are similarly dominated by detrital clay minerals (illite/chlorite), with minor quantities of authigenic kaolinite and smectite (Chamley et al., 1993). Measured Na/Cl ratios of stream waters from Susquehanna Shale Hills Critical Zone Observatory are centered around 1, with little to no excess sodium (Na*; (Brantley, 2024). The erosion rate of Susquehanna Shale Hills is over 3 orders of magnitude slower than that of the Taiwanese or Himalayan catchments (8 to 29 μm yr^{-1}; Jin et al., 2010). Consequently, no meaningful addition of recycled sodium via desorption is expected (Fig. 7). Within the Mackenzie Basin, excesses in sodium to chloride are observed within all regions of the watershed; however, rivers draining uplifted marine sediments are found to have lower Na*/Si ratios than those of other regions (Rocky and Mackenzie mountains: 1.2 ± 0.8 (N = 34); interior platform: 6.5 ± 8.3 (N = 17); transition mountain/plain: 3.1 ± 2.2 (N = 9); Canadian Shield: 23.4 ± 40 (N = 11); Millot et al., 2003). Instead, Na*/Si ratios of rivers are at their greatest within the Canadian Shield where sodium desorption and geothermal water inputs are less likely. This suggests the relationship between erosion (E), marine sodium desorption (Na_{de}), and Na*/Si ratios is complex and further work to understand the fate of adsorbed marine elements during burial and uplift would be beneficial for understanding both the potential bias to silicate weathering rates and the geological cycling of adsorbed species.

4.3.3. Other potential drivers of increased Na*/Si ratios

The non-stoichiometric preferential release of alkali and alkali-earth cations (including sodium) during the dissolution of silicate minerals provides a third potential process to explain the Na*/Si ratios. This has been observed in the early stages of plagioclase dissolution in laboratory experiments (Stillings and Brantley, 1995); however, no concomitant depletion in the Na/Si of plagioclases in the study catchments has been observed. The uptake of dissolved silicon by vascular land plants also provides a potential driver for the enrichment (Fulweiler and Nixon, 2005). The export of biomass (required for the year-round elevation of Na*/Si ratios) is thought to be particularly important in highly erosive regions (Frings et al., 2021). For biological uptake and export to explain the observed hysteresis in dissolved silicon (Fig. 5), a decrease in either the uptake of dissolved silicon or efficiency of export during maximal discharge is required. This is not the expected seasonal behaviour; however, further work monitoring the export of biogenic silica on a seasonal basis is necessary to explore this hypothesis. Non-chloride sodium-bearing salts ($NaHCO_3$, Na_2CO_3, NaCl, Na_2SO_4, and $NaNO_3$) provide another potential driver of increased Na*/Si ratios. Alkaline salts present within the endorheic floodplain and peninsular sub-basin soils of the Ganges-Brahmaputra watershed can significantly increase the dissolved sodium concentration of the rivers (Chatterjee and Singh, 2022). The formation of these highly-soluble salts from low-ionic strength river waters requires extensive evaporation of large static water bodies (Monnin and Schott, 1984). Alkaline salts are therefore an unlikely driver of the increased Na*/Si ratios observed within the steeply inclined, exorheic, catchments of this study.

4.4. The importance of understanding hydrothermal weathering reactions for the relationship between tectonics and climate

The precipitation of secondary silicate minerals provides a key limitation to the efficiency of silicate weathering. The type of minerals formed and their relationship with climate is therefore important for understanding carbon cycle feedbacks. The clay mineralogy of US shale catchments was found to vary depending on the humidity index (HI), interpreted as a runoff limitation (Shaughnessy and Brantley, 2023). This demonstrates a climatic control on silicate weathering and the carbon cycle. Within the catchments of uplifted siliclastic sedimentary units (e.g., Himalayas, Taiwan, Andes) detrital minerals (notably illite) dominate the clay mineral assemblage (Huyghe et al., 2011; Chamley et al., 1993; Guyot et al., 2007). The hydrothermal illitisation of smectite (I/S) during diagenesis of marine sediments has been observed in the field and the laboratory (Meunier et al., 2004). During this process, smectites (expandable; CEC between 60 to 120 meq/100 g; hydrated inter-layer cations including sodium) are gradually replaced by illites (non-expandable, CEC ~25 meq 100 g^{-1}, inter-layer mostly-fixed potassium ions). This process results in the desorption of adsorbed cations and expulsion of inter-layer water (Mosser-Ruck et al., 2001). Extensive illitisation of smectites is proposed as an explanation for the abundance of illite in the clay mineral fraction of Himalayan sediments (Huyghe et al., 2011; Vögeli et al., 2017). This process therefore has the potential to explain increases in Na/Cl through the desorption of adsorbed marine sodium, but requires further precipitation of Si-rich minerals to explain the Na*/Si of hot spring geothermal waters. The observations of mobile riverine chemistry and mineralogy from the catchments of this study demonstrate the importance of sub-surface hydrothermal processes in highly erosive meta-sedimentary catchments, in agreement with the results of Evans et al. (2004) and Calmels et al. (2011). This study also reinforces the conclusions of other studies which demonstrate the complex relationship between mountain uplift, the carbon cycle and climate (Jacobson and Blum, 2003; Moore et al., 2013; Li et al., 2014; Zondervan et al., 2023; Erlanger et al., 2024). Further research utilising isotopic tracers of silicate mineral precipitation-dissolution reactions (lithium and silicon stable isotope ratios) may provide unique insights into the link between hydrothermal weathering processes and climate.

5. Conclusions

The fluxes of dissolved and adsorbed cations from three large Himalayan rivers were measured over a period of two years to determine the impact of adsorption-desorption reactions on river chemistry and chemical weathering rates. Precipitation-driven increases in suspended

sediment concentrations, discharge, and the cation exchange capacity (CEC) of sediment during the monsoon resulted in adsorbed cation fluxes varying by over 3 orders of magnitude between the seasons. During the monsoon, significant proportions of mobile calcium (21%), strontium (23%) and barium (71%) are transported adsorbed to the sediment. Despite the seasonal variability, the partitioning of cations between the adsorbed and dissolved phases followed a consistent order across all samples measured (greatest proportion adsorbed: Ba > Sr & Ca > K & Mg > Na). Episodic extreme sediment concentration events were responsible for transporting up to 13% of the annual sediment and adsorbed cation fluxes, highlighting the importance of these rarely sampled events for global biogeochemical cycles. The ratio of excess sodium (Na* = Na-Cl) to dissolved silicon (Si) has previously been attributed to reflect different surficial weathering regimes. The mixing of geothermal waters from hot springs (localised along the Main Central Thrust) with surface waters provides the most likely driver of the annual variability in Na*/Si ratios observed. The desorption of old marine sodium from uplifted marine sediments provides a potential driver of the increased Na*/Si ratios. Accounting for the excess sodium reduces conventional silicate weathering rate estimates by up to 83% in the catchments.

CRediT authorship contribution statement

Alasdair C.G. Knight: Writing – review & editing, Writing – original draft, Visualization, Methodology, Investigation, Formal analysis, Data curation, Conceptualization. **Emily I. Stevenson:** Writing – review & editing, Writing – original draft. **Luke Bridgestock:** Writing – review & editing, Writing – original draft. **J. Jotautas Baronas:** Writing – review & editing, Writing – original draft. **William J. Knapp:** Writing – review & editing. **Basanta Raj Adhikari:** Writing – review & editing. **Christoff Andermann:** Writing – review & editing, Writing – original draft, Data curation. **Edward T. Tipper:** Writing – review & editing, Writing – original draft, Methodology, Investigation, Conceptualization.

Declaration of competing interest

The authors declare that they have no known competing financial interests or personal relationships that could have appeared to influence the work reported in this paper.

Data availability

Discharge, suspended sediment concentrations, and dissolved ion concentrations for the Narayani River are sourced from Märki et al. (2021) and Morin et al. (2018). Discharge measurements for the Saptakoshi and Sunkoshi were made by the Department of Hydrology and Meteorology in Nepal (DHM). Adsorbed and dissolved element concentrations for the Saptakoshi and Sunkoshi rivers are available at https://doi.org/10.5880/fidgeo.2024.008. Suspended sediment concentrations are available at https://doi.org/10.5880/GFZ.4.6.2023.001.

Acknowledgements

The manuscript benefitted from the reviews of two anonymous reviewers. M.J.B. is thanked for his thoughtful questions and insightful comments throughout this study. A.K. was supported by a NERC DTP studentship (NE/S007164/1). This study would not have been successful without the continual assistance and guidance of Marie-Laure Bagard and Heye Freymuth in the laboratories at the Department of Earth Sciences, University of Cambridge. This work was funded by the NERC grant NE/T007214/1.

Appendix A. Supplementary material

Supplementary material related to this article can be found online at https://doi.org/10.1016/j.epsl.2024.118814.

References

Andermann, C., Crave, A., Gloaguen, R., Davy, P., Bonnet, S., 2012. Connecting source and transport: suspended sediments in the Nepal Himalayas. Earth Planet. Sci. Lett. 351–352, 158–170. https://doi.org/10.1016/j.epsl.2012.06.059. https://www.sciencedirect.com/science/article/pii/S0012821X12003512.

Appelo, C.A., Postma, D., 2005. Geochemistry, Groundwater and Pollution, 2 ed. CRC Press.

Appelo, C.A.J., 1996. Multicomponent ion exchange and chromatography in natural systems. In: Reactive Transport in Porous Media, pp. 193–228. https://www.degruyter.com/document/doi/10.1515/9781501509797-007/html.

Aran, D., Maul, A., Masfaraud, J.F., 2008. A spectrophotometric measurement of soil cation exchange capacity based on cobaltihexamine chloride absorbance. C. R. Géosci. 340, 865–871. https://doi.org/10.1016/j.crte.2008.07.015. https://www.sciencedirect.com/science/article/pii/S1631071308001910.

Becker, J.A., Bickle, M.J., Galy, A., Holland, T.J.B., 2008. Himalayan metamorphic CO2 fluxes: quantitative constraints from hydrothermal springs. Earth Planet. Sci. Lett. 265, 616–629. https://doi.org/10.1016/j.epsl.2007.10.046. https://www.sciencedirect.com/science/article/pii/S0012821X07007091.

Berner, R.A., 1990. Atmospheric carbon dioxide levels over Phanerozoic time. Science 249, 1382–1386. https://doi.org/10.1126/science.249.4975.1382.

Bickle, M.J., Chapman, H.J., Bunbury, J., Harris, N.B.W., Fairchild, I.J., Ahmad, T., Pomiès, C., 2005. Relative contributions of silicate and carbonate rocks to riverine Sr fluxes in the headwaters of the Ganges. Geochim. Cosmochim. Acta 69, 2221–2240. https://doi.org/10.1016/j.gca.2004.11.019. http://www.sciencedirect.com/science/article/pii/S001670370400955X.

Bouchez, J., Moquet, J.S., Espinoza, J.C., Martinez, J.M., Guyot, J.L., Lagane, C., Filizola, N., Noriega, L., Hidalgo Sanchez, L., Pombosa, R., 2017. River mixing in the Amazon as a driver of concentration-discharge relationships. Water Resour. Res. 53, 8660–8685. https://doi.org/10.1002/2017WR020591. https://onlinelibrary.wiley.com/doi/abs/10.1002/2017WR020591.

Brantley, S.L., 2024. SSHCZO – Stream Water Chemistry, Groundwater Chemistry – Shale Hills – (2008-2010).

Brantley, S.L., Shaughnessy, A., Lebedeva, M.I., Balashov, V.N., 2023. How temperature-dependent silicate weathering acts as Earth's geological thermostat. Science 379, 382–389. https://doi.org/10.1126/science.add2922. https://www.science.org/doi/full/10.1126/science.add2922.

Bufe, A., Hovius, N., Emberson, R., Rugenstein, J.K.C., Galy, A., Hassenruck-Gudipati, H.J., Chang, J.M., 2021. Co-variation of silicate, carbonate and sulfide weathering drives CO2 release with erosion. Nat. Geosci. 14, 211–216. https://doi.org/10.1038/s41561-021-00714-3. https://www.nature.com/articles/s41561-021-00714-3.

Calmels, D., Galy, A., Hovius, N., Bickle, M., West, A.J., Chen, M.C., Chapman, H., 2011. Contribution of deep groundwater to the weathering budget in a rapidly eroding mountain belt, Taiwan. Earth Planet. Sci. Lett. 303, 48–58.

Campbell, F.A., Williams, G.D., 1965. Chemical composition of shales of Mannville group (Lower Cretaceous) of central Alberta, Canada. Am. Assoc. Pet. Geol. Bull. 49, 81–87. https://doi.org/10.1306/A66334EA-16C0-11D7-8645000102C1865D.

Cerling, T.E., Pederson, B.L., Damm, K.L.V., 1989. Sodium-calcium ion exchange in the weathering of shales: implications for global weathering budgets. Geology 17, 552–554. https://doi.org/10.1130/0091-7613(1989)017<0552:SCIEIT>2.3.CO;2. https://pubs.geoscienceworld.org/geology/article/17/6/552/204924/Sodium-calcium-ion-exchange-in-the-weathering-of.

Chamley, H., Angelier, J., Teng, L.S., 1993. Tectonic and environmental control of the clay mineral sedimentation in the late Cenozoic orogen of Taiwan. Geodin. Acta 6, 135–147. https://doi.org/10.1080/09853111.1993.11105243.

Chatterjee, J., Singh, S.K., 2022. Impact of dissolution of Saline-Alkaline soils on the hydrochemistry and erosion rates of the Ganga river system. Geochem. Geophys. Geosyst. 23, e2021GC009914. https://doi.org/10.1029/2021GC009914. https://onlinelibrary.wiley.com/doi/abs/10.1029/2021GC009914.

Cook, K.L., Andermann, C., Gimbert, F., Adhikari, B.R., Hovius, N., 2018. Glacial lake outburst floods as drivers of fluvial erosion in the Himalaya. Science 362, 53–57. https://doi.org/10.1126/science.aat4981. https://www.science.org/doi/full/10.1126/science.aat4981.

Dadson, S.J., Hovius, N., Chen, H., Dade, W.B., Hsieh, M.L., Willett, S.D., Hu, J.C., Horng, M.J., Chen, M.C., Stark, C.P., Lague, D., Lin, J.C., 2003. Links between erosion, runoff variability and seismicity in the Taiwan orogen. Nature 426, 648–651. https://doi.org/10.1038/nature02150. https://www.nature.com/articles/nature02150.

De Segonzac, G.D., 1970. The transformation of clay minerals during diagenesis and low-grade metamorphism: a review. Sedimentology 15, 281–346. https://doi.org/10.1111/j.1365-3091.1970.tb02190.x. https://onlinelibrary.wiley.com/doi/abs/10.1111/j.1365-3091.1970.tb02190.x.

Dellinger, M., Gaillardet, J., Bouchez, J., Calmels, D., Galy, V., Hilton, R.G., Louvat, P., France-Lanord, C., 2014. Lithium isotopes in large rivers reveal the cannibalistic nature of modern continental weathering and erosion. Earth Planet. Sci. Lett. 401, 359–372. https://doi.org/10.1016/j.epsl.2014.05.061. http://www.sciencedirect.com/science/article/pii/S0012821X14003793.

Dethier, E.N., Renshaw, C.E., Magilligan, F.J., 2022. Rapid changes to global river suspended sediment flux by humans. Science 376, 1447–1452. https://doi.org/10.1126/science.abn7980. https://www.science.org/doi/full/10.1126/science.abn7980.

Ebelmen, J.J., 1845. Sur les produits de la décomposition des espèces minérales de la famille des silicates. Ann. Mines 7, 3–66.

Erlanger, E., Bufe, A., Paris, G., D'Angeli, I., Pisani, L., Kemeny, P.C., Stammeier, J., Haghipour, N., Hovius, N., 2024. Deep CO2 release and the carbon budget of the central Apennines modulated by geodynamics. Nat. Geosci., 1–7. https://doi.org/10.1038/s41561-024-01396-3. https://www.nature.com/articles/s41561-024-01396-3.

Evans, M.J., Derry, L.A., France-Lanord, C., 2004. Geothermal fluxes of alkalinity in the Narayani river system of central Nepal. Geochem. Geophys. Geosyst. 5. https://doi.org/10.1029/2004GC000719. https://onlinelibrary.wiley.com/doi/abs/10.1029/2004GC000719, 2004.

Favre, F., Tessier, D., Abdelmoula, M., Génin, J.M., Gates, W.P., Boivin, P., 2002. Iron reduction and changes in cation exchange capacity in intermittently waterlogged soil. Eur. J. Soil Sci. 53, 175–183. https://doi.org/10.1046/j.1365-2389.2002.00423.x. https://onlinelibrary.wiley.com/doi/abs/10.1046/j.1365-2389.2002.00423.x.

Fitzsimons, S.J., Veit, H., 2001. Geology and geomorphology of the European Alps and the southern Alps of New Zealand. Mt. Res. Dev. 21, 340–349. https://doi.org/10.1659/0276-4741(2001)021[0340:GAGOTE]2.0.CO;2. https://bioone.org/journals/mountain-research-and-development/volume-21/issue-4/0276-4741_2001_021_0340_GAGOTE_2.0.CO_2/Geology-and-Geomorphology-of-the-European-Alps-and-the-Southern/10.1659/0276-4741(2001)021[0340:GAGOTE]2.0.CO;2.full.

Frings, P.J., Schubring, F., Oelze, M., Von Blanckenburg, F., 2021. Quantifying biotic and abiotic Si fluxes in the Critical Zone with Ge/Si ratios along a gradient of erosion rates. Am. J. Sci. 321, 1204–1245. https://doi.org/10.2475/08.2021.03. https://ajsonline.org/article/65829.

Fulweiler, R.W., Nixon, S.W., 2005. Terrestrial vegetation and the seasonal cycle of dissolved silica in a southern New England coastal river. Biogeochemistry 74, 115–130. https://doi.org/10.1007/s10533-004-2947-z.

Gaillardet, J., Dupré, B., Louvat, P., Allègre, C.J., 1999. Global silicate weathering and CO2 consumption rates deduced from the chemistry of large rivers. Chem. Geol. 159, 3–30. https://doi.org/10.1016/S0009-2541(99)00031-5. http://www.sciencedirect.com/science/article/pii/S0009254199000315.

Gaines Jr., G.L., Thomas, H.C., 1953. Adsorption studies on clay minerals. II. A formulation of the thermodynamics of exchange adsorption. Z. Chem. Phys. 21, 714–718. https://doi.org/10.1063/1.1698996.

Galy, A., France-Lanord, C., 1999. Weathering processes in the Ganges–Brahmaputra basin and the riverine alkalinity budget. Chem. Geol. 159, 31–60. https://doi.org/10.1016/S0009-2541(99)00033-9. https://www.sciencedirect.com/science/article/pii/S0009254199000339.

Galy, A., France-Lanord, C., 2001. Higher erosion rates in the Himalaya: geochemical constraints on riverine fluxes. Geology 29, 23–26. https://doi.org/10.1130/0091-7613(2001)029<0023:HERITH>2.0.CO;2.

Guyot, J.L., Jouanneau, J.M., Soares, L., Boaventura, G.R., Maillet, N., Lagane, C., 2007. Clay mineral composition of river sediments in the Amazon basin. Catena 71, 340–356. https://doi.org/10.1016/j.catena.2007.02.002. https://www.sciencedirect.com/science/article/pii/S0341816207000355.

Hartmann, J., Jansen, N., Dürr, H.H., Kempe, S., Köhler, P., 2009. Global CO2-consumption by chemical weathering: what is the contribution of highly active weathering regions? Glob. Planet. Change 69, 185–194. https://doi.org/10.1016/j.gloplacha.2009.07.007. https://www.sciencedirect.com/science/article/pii/S0921818109001349.

Hartmann, J., Lauerwald, R., Moosdorf, N., 2019. GLORICH - Global river chemistry database.

Horton, B.K., 2018. Sedimentary record of Andean mountain building. Earth-Sci. Rev. 178, 279–309. https://doi.org/10.1016/j.earscirev.2017.11.025. https://www.sciencedirect.com/science/article/pii/S0012825217304300.

Hou, Z., Duan, L., Lu, Y., Zheng, Y., Zhu, D., Yang, Z., Yang, Z., Wang, B., Pei, Y., Zhao, Z., McCuaig, T.C., 2015. Lithospheric architecture of the Lhasa terrane and its control on ore deposits in the Himalayan-Tibetan orogen. Econ. Geol. 110, 1541–1575. https://doi.org/10.2113/econgeo.110.6.1541.

Huyghe, P., Guilbaud, R., Bernet, M., Galy, A., Gajurel, A.P., 2011. Significance of the clay mineral distribution in fluvial sediments of the Neogene to Recent Himalayan Foreland Basin (west-central Nepal). Basin Res. 23, 332–345. https://doi.org/10.1111/j.1365-2117.2010.00485.x. https://www.earthdoc.org/content/journals/10.1111/j.1365-2117.2010.00485.x.

Jacobson, A.D., Blum, J.D., 2003. Relationship between mechanical erosion and atmospheric CO2 consumption in the New Zealand Southern Alps. Geology 31, 865–868. https://doi.org/10.1130/G19662.1.

Jang, C.S., Chen, J.S., Lin, Y.B., Liu, C.W., 2012. Characterizing hydrochemical properties of springs in Taiwan based on their geological origins. Environ. Monit. Assess. 184, 63–75. https://doi.org/10.1007/s10661-011-1947-4.

Jin, L., Ravella, R., Ketchum, B., Bierman, P.R., Heaney, P., White, T., Brantley, S.L., 2010. Mineral weathering and elemental transport during hillslope evolution at the Susquehanna/Shale Hills Critical Zone Observatory. Geochim. Cosmochim. Acta 74, 3669–3691. https://doi.org/10.1016/J.GCA.2010.03.036.

Li, D.D., Jacobson, A.D., McInerney, D.J., 2014. A reactive-transport model for examining tectonic and climatic controls on chemical weathering and atmospheric CO2 consumption in granitic regolith. Chem. Geol. 365, 30–42. https://doi.org/10.1016/j.chemgeo.2013.11.028. https://www.sciencedirect.com/science/article/pii/S0009254113005664.

Lupker, M., Blard, P.H., Lavé, J., France-Lanord, C., Leanni, L., Puchol, N., Charreau, J., Bourlès, D., 2012. 10Be-derived Himalayan denudation rates and sediment budgets in the Ganga basin. Earth Planet. Sci. Lett. 333–334, 146–156. https://doi.org/10.1016/j.epsl.2012.04.020. https://www.sciencedirect.com/science/article/pii/S0012821X12001872.

Lupker, M., France-Lanord, C., Lartiges, B., 2016. Impact of sediment–seawater cation exchange on Himalayan chemical weathering fluxes. Earth Surf. Dyn. 4, 675–684. https://doi.org/10.3929/ethz-b-000119685. https://www.research-collection.ethz.ch/handle/20.500.11850/119685.

Märki, L., Lupker, M., France-Lanord, C., Lavé, J., Gallen, S., Gajurel, A.P., Haghipour, N., Leuenberger-West, F., Eglinton, T., 2021. An unshakable carbon budget for the Himalaya. Nat. Geosci. 14 (10), 745–750. https://doi.org/10.1038/s41561-021-00815-z. https://www.nature.com/articles/s41561-021-00815-z.

Meunier, A., Velde, B., Velde, B., 2004. Illite: Origins, Evolution and Metamorphism. Springer Science & Business Media.

Milliman, J.D., Farnsworth, K.L., 2013. River Discharge to the Coastal Ocean: A Global Synthesis. Cambridge University Press. https://www.cambridge.org/in/universitypress/subjects/earth-and-environmental-science/geomorphology-and-physical-geography/river-discharge-coastal-ocean-global-synthesis.

Millot, R., Gaillardet, J., Dupré, B., Allègre, C.J., 2003. Northern latitude chemical weathering rates: clues from the Mackenzie river basin, Canada. Geochim. Cosmochim. Acta 67, 1305–1329. https://doi.org/10.1016/S0016-7037(02)01207-3. https://www.sciencedirect.com/science/article/pii/S0016703702012073.

Monnin, C., Schott, J., 1984. Determination of the solubility products of sodium carbonate minerals and an application to trona deposition in Lake Magadi (Kenya). Geochim. Cosmochim. Acta 48, 571–581. https://doi.org/10.1016/0016-7037(84)90285-0. https://www.sciencedirect.com/science/article/pii/0016703784902850.

Montgomery, D.R., Brandon, M.T., 2002. Topographic controls on erosion rates in tectonically active mountain ranges. Earth Planet. Sci. Lett. 201, 481–489. https://doi.org/10.1016/S0012-821X(02)00725-2. https://www.sciencedirect.com/science/article/pii/S0012821X02007252.

Moon, S., Chamberlain, C.P., Hilley, G.E., 2014. New estimates of silicate weathering rates and their uncertainties in global rivers. Geochim. Cosmochim. Acta 134, 257–274. https://doi.org/10.1016/j.gca.2014.02.033. https://www.sciencedirect.com/science/article/pii/S0016703714001422.

Moore, J., Jacobson, A.D., Holmden, C., Craw, D., 2013. Tracking the relationship between mountain uplift, silicate weathering, and long-term CO2 consumption with Ca isotopes: Southern Alps, New Zealand. Chem. Geol. 341, 110–127. https://doi.org/10.1016/j.chemgeo.2013.01.005. https://www.sciencedirect.com/science/article/pii/S0009254113000338.

Morin, G.P., Lavé, J., France-Lanord, C., Rigaudier, T., Gajurel, A.P., Sinha, R., 2018. Annual sediment transport dynamics in the Narayani basin, central Nepal: assessing the impacts of erosion processes in the annual sediment budget. J. Geophys. Res., Earth Surf. 123, 2341–2376. https://doi.org/10.1029/2017JF004460. https://onlinelibrary.wiley.com/doi/abs/10.1029/2017JF004460.

Mosser-Ruck, R., Pironon, J., Cathelineau, M., Trouiller, A., 2001. Experimental illitization of smectite in a K-rich solution. Eur. J. Mineral. 13, 829–840. https://doi.org/10.1127/0935-1221/2001/0013-0829.

Oliver, L., Harris, N., Bickle, M., Chapman, H., Dise, N., Horstwood, M., 2003. Silicate weathering rates decoupled from the 87Sr/86Sr ratio of the dissolved load during Himalayan erosion. Chem. Geol. 201, 119–139. https://doi.org/10.1016/S0009-2541(03)00236-5. https://www.sciencedirect.com/science/article/pii/S0009254103002365.

Price, J.R., Velbel, M.A., Patino, L.C., 2005. Rates and time scales of clay-mineral formation by weathering in saprolitic regoliths of the southern Appalachians from geochemical mass balance. Geol. Soc. Am. Bull. 117, 783–794. https://doi.org/10.1130/B25547.1.

Raymo, M., Ruddiman, W., 1992. Tectonic forcing of late Cenozoic climate. Nature 359, 117–122. https://doi.org/10.1038/359117a0.

Saidian, M., Godinez, L.J., Prasad, M., 2016. Effect of clay and organic matter on nitrogen adsorption specific surface area and cation exchange capacity in shales (mudrocks). J. Nat. Gas Sci. Eng. 33, 1095–1106. https://doi.org/10.1016/j.jngse.2016.05.064. https://www.sciencedirect.com/science/article/pii/S187551001630378X.

Samanta, S., Dalai, T.K., 2016. Dissolved and particulate Barium in the Ganga (Hooghly) river estuary, India: solute-particle interactions and the enhanced dissolved flux to the oceans. Geochim. Cosmochim. Acta 195, 1–28. https://doi.org/10.1016/j.gca.2016.09.005. http://www.sciencedirect.com/science/article/pii/S001670371630518X.

Sayles, F.L., Mangelsdorf, P.C., 1977. The equilibration of clay minerals with sea water: exchange reactions. Geochim. Cosmochim. Acta 41, 951–960. https://doi.org/10.1016/0016-7037(77)90154-5. http://www.sciencedirect.com/science/article/pii/0016703777901545.

Sayles, F.L., Mangelsdorf, P.C., 1979. Cation-exchange characteristics of Amazon River suspended sediment and its reaction with seawater. Geochim. Cosmochim. Acta 43, 767–779. https://doi.org/10.1016/0016-7037(79)90260-6. http://www.sciencedirect.com/science/article/pii/0016703779902606.

Shaughnessy, A.R., Brantley, S.L., 2023. How do silicate weathering rates in shales respond to climate and erosion? Chem. Geol. 629, 121474. https://doi.org/10.1016/j.chemgeo.2023.121474. https://www.sciencedirect.com/science/article/pii/S0009254123001742.

Sparks, D.L., 1986. Kinetics of ionic reactions in clay minerals and soils. In: Brady, N.C. (Ed.), Advances in Agronomy, vol. 38. Academic Press, pp. 231–266. https://www.sciencedirect.com/science/article/pii/S006521130860677X.

Sparks, D.L., Page, A.L., Loeppert, R.H., 2020. Chemical methods. In: Methods of Soil Analysis. Soil Science Society of America, p. 1424.

Stallard, R., Edmond, J., 1987. Geochemistry of the Amazon: 3. Weathering chemistry and limits to dissolved inputs. J. Geophys. Res., Oceans 92, 8293–8302. https://doi.org/10.1029/JC092iC08p08293. https://onlinelibrary.wiley.com/doi/abs/10.1029/JC092iC08p08293.

Stillings, L.L., Brantley, S.L., 1995. Feldspar dissolution at 25 °C and pH 3: reaction stoichiometry and the effect of cations. Geochim. Cosmochim. Acta 59, 1483–1496. https://doi.org/10.1016/0016-7037(95)00057-7. https://www.sciencedirect.com/science/article/pii/0016703795000577.

Tang, L., Sparks, D.L., 1993. Cation-exchange kinetics on montmorillonite using pressure-jump relaxation. Soil Sci. Soc. Am. J. 57, 42–46. https://doi.org/10.2136/SSSAJ1993.03615995005700010009X. https://onlinelibrary.wiley.com/doi/full/10.2136/sssaj1993.03615995005700010009x.

Tipper, E.T., Stevenson, E.I., Alcock, V., Knight, A.C., Baronas, J.J., Hilton, R.G., Bickle, M.J., Larkin, C.S., Feng, L., Relph, K.E., Hughes, G., 2020. Global silicate weathering flux overestimated because of sediment-water cation exchange. Proc. Natl. Acad. Sci. USA 118. https://doi.org/10.1073/PNAS.2016430118/-/DCSUPPLEMENTAL.

Townsend, R.P., Fowden, L., Barrer, R.M., Tinker, P.B., 1984. Thermodynamics of ion exchange in clays. Philos. Trans. R. Soc. Lond. Ser. A, Math. Phys. Sci. 311, 301–314. https://doi.org/10.1098/rsta.1984.0030. https://royalsocietypublishing.org/doi/10.1098/rsta.1984.0030.

Vögeli, N., van der Beek, P., Huyghe, P., Najman, Y., 2017. Weathering in the Himalaya, an East-West comparison: indications from major elements and clay mineralogy. J. Geol. 125, 515–529. https://www.jstor.org/stable/26547019.

West, A.J., Galy, A., Bickle, M., 2005. Tectonic and climatic controls on silicate weathering. Earth Planet. Sci. Lett. 235, 211–228. https://doi.org/10.1016/j.epsl.2005.03.020. https://www.sciencedirect.com/science/article/pii/S0012821X05002116.

White, A.F., Brantley, S.L., 2003. The effect of time on the weathering of silicate minerals: why do weathering rates differ in the laboratory and field? Chem. Geol. 202, 479–506. https://doi.org/10.1016/j.chemgeo.2003.03.001. https://www.sciencedirect.com/science/article/pii/S0009254103002560.

White, A.F., Schulz, M.S., Stonestrom, D.A., Vivit, D.V., Fitzpatrick, J., Bullen, T.D., Maher, K., Blum, A.E., 2009. Chemical weathering of a marine terrace chronosequence, Santa Cruz, California. Part II: solute profiles, gradients and the comparisons of contemporary and long-term weathering rates. Geochim. Cosmochim. Acta 73, 2769–2803. https://doi.org/10.1016/j.gca.2009.01.029. http://www.sciencedirect.com/science/article/pii/S0016703709000787.

Wittmann, H., Oelze, M., Gaillardet, J., Garzanti, E., von Blanckenburg, F., 2020. A global rate of denudation from cosmogenic nuclides in the Earth's largest rivers. Earth-Sci. Rev. 204, 103147. https://doi.org/10.1016/j.earscirev.2020.103147. https://www.sciencedirect.com/science/article/pii/S0012825219304039.

Yin, A., 2006. Cenozoic tectonic evolution of the Himalayan orogen as constrained by along-strike variation of structural geometry, exhumation history, and foreland sedimentation. Earth-Sci. Rev. 76, 1–131. https://doi.org/10.1016/j.earscirev.2005.05.004. https://www.sciencedirect.com/science/article/pii/S0012825205000565.

Yin, A., Harrison, T.M., 2000. Geologic evolution of the Himalayan-Tibetan orogen. Annu. Rev. Earth Planet. Sci. 28, 211–280. https://doi.org/10.1146/annurev.earth.28.1.211. https://www.annualreviews.org/content/journals/10.1146/annurev.earth.28.1.211.

Zaytseva, E., 1958. Cation exchange capacity of marine sediments and methods of determination. Tr. Inst. Okeanol., Akad. Nauk SSSR 46, 181–204.

Zondervan, J.R., Hilton, R.G., Dellinger, M., Clubb, F.J., Roylands, T., Ogrič, M., 2023. Rock organic carbon oxidation CO2 release offsets silicate weathering sink. Nature, 1–5. https://doi.org/10.1038/s41586-023-06581-9. https://www.nature.com/articles/s41586-023-06581-9.